Single cell gene fusion detection by scFusion

Zijie Jin[a]; Wenjian Huang[b]; Ning Shen[c]; Juan Li [d]; Xiaochen Wang[a]; Peter J. Park[c]; Ruibin Xi [a,e,*].

a. School of Mathematical Sciences, Peking University, Beijing, 100871, China;
b. Academy for Advanced Interdisciplinary Studies, Peking University, Beijing, 100871, China;
c. Department of Biomedical Informatics, Harvard Medical School, Boston, MA, 02115, USA;
d. Department of Biomedical Engineering, College of Engineering, Peking University, Beijing, 100871, China;
e. Center for Statistical Science, Peking University, Beijing,100871, China.

Significance

A critical challenge for fusion detection based on the full-length single cell RNA sequencing (scRNA-seq) is to identify the needles, or the true fusions, from a large haystack of false positives. We developed a fusion detection tool scFusion for scRNA-seq. scFusion is computationally more efficient, has far less false discoveries while achieves similar detection power compared to fusion detection tools developed for bulk data. Application of scFusion to a multiple myeloma dataset identied subclones with the fusion *IgH-WHSC1* and revealed that over-expression of the oncogene *WHSC1* was strongly associated with the fusion. The models developed in this work may also be generalized for other single cell analyses such as structural variation detection and the alternative splicing analysis.

Abstract

Gene fusions are widespread in tumor cells and can play important roles in tumor initiation and progression. Using full length single cell RNA sequencing (scRNA-seq), gene fusions can now be detected at single cell level by analyzing chimeric reads in scRNA-seq. However, scRNA-seq data has a high noise level and contains various technical artefacts. Direct application of fusion detection tools developed for bulk data can lead to spurious fusion discoveries and leave some true fusions undetected. In this paper, we present a computational tool, scFusion, for gene fusion detection based on scRNA-seq. scFusion is composed of a statistical model and a deep learning model, both of which are designed to control for potential false discoveries. The statistical model models the background noise as zero inflated negative binomial and uses a statistical testing procedure to control for false positives. The deep learning model is trained to recognize technical chimeric artefacts and filter false fusion candidates generated by these artefacts. We compared scFusion with bulk fusion detection methods using simulation data created based on real scRNA-seq data and found that scFusion had superior performance. Applying scFusion to a T cell data, scFusion successfully detected the invariant TCR gene recombinations in Mucosal-associated invariant T cells that many bulk methods failed to detect. In a multiple myeloma data,

scFusion detected the known recurrent fusion *IgH-WHSC1,* which was associated with overexpression of the *WHSC1* oncogene.

Introduction

Gene fusions are hybrid genes by joining of two independent genes, often resulting from structural rearrangements such as deletions and translocations(1). In cancer cells, many gene fusions are driver mutations that play important roles in the carcinogenesis process. Well-known examples include the *BCR–ABL1* fusion in chronic myeloid leukemia(2), the *TMPRSS2–ERG* fusion in prostate cancer(3) and the *ALK* fusions in lung cancer(4). Some gene fusions are strongly correlated with tumor subtypes and are often used as diagnostic markers for malignancy. Gene fusions are also important targets of cancer drugs. A number of such drugs have been approved by the US Food and Drug Administration such as imatinib targeting *BCR-ABL1*(5), crizotinib targeting *ALK* fusions(6) and the recently approved TRK inhibitor larotrectinib targeting *NTRK* fusions(7).

RNA sequencing (RNA-seq) provides an accurate and unbiased platform for gene fusion detection. Gene fusions generate chimeric reads that cover junctions of independent partner genes. After mapping, these chimeric reads will be split-aligned to the partner genes and gene fusions can be detected. The development of full length single cell RNA sequencing (scRNA-seq) (8-10) unprecedentedly enables the detection and investigation of gene fusions at single cell level. Fusion detection at single cell level could allow identification of cell subtypes or subclones that play unique roles in the complex biological systems and/or have unique phenotypic, genotypic and transcriptomic features. However, although many computational fusion detection tools have been developed for bulk RNA-seq data(11-19), to the best of our knowledge, no fusion detection method is available for scRNA-seq data. Direct application of bulk RNA-seq fusion detection methods to scRNA-seq may have limited performance: (1) The heavy amplification step of scRNA-seq may generate artifacial chimeric reads and lead to false positive gene fusion discoveries; (2) Bulk methods, when applied to scRNA-seq data, detect gene fusions for each single cell independently. The power for detecting fusions shared among multiple single cells can be improved if all single cells are integratively analyzed. (3) Current single cell data often contain thousands or even more single cells. Although one cell's data is generally smaller than a bulk RNA-seq data, collectively, scRNA-seq data is large. Many bulk methods are not optimized for this setup and can be computationally expensive.

In this paper, we developed a gene fusion detection algorithm named scFusion based on the full length scRNA-seq data. scFusion takes full advantage of all single cell data for fusion detection by combining two independent models. First, scFusion builds an integrative statistical model of all supporting chimeric reads. Then a deep learning model is applied to filter out fusion candidates potentially caused by technical artefacts. To assess the performance of scFusion, we first simulated single cell data on the basis of real scRNA-seq data. Compared to bulk fusion detection methods, scFusion achieved high sensitivity while maintaining a low false discovery rate (FDR). Next, we experimentally added gene fusions to single cells and validated that scFusion could successfully detect these spike-in fusions. Finally, we applied scFusion to two publicly available scRNA-seq data and found that scFusion outperformed bulk methods.

Results

scFusion is a method designed to detect gene fusion from scRNA-seq data

scFusion takes input as reads mapped by STAR(20) (Figure 1). Uniquely split-mapped reads and discordant reads mapped to different genes are identified and clustered to obtain candidate gene fusion list. After filtering fusion candidates in pseudogenes, long noncoding RNAs (lncRNAs), genes without an approved symbol (21) (such as *RP11-475J5.6*), and in the intronic regions, we observed well over 10,000 fusion candidates in all datasets tested (Figure S1). When considering only candidates found in at least two cells, there were still thousands of fusion candidates, which were mainly false positives. For example, the T cells of a hepatocarcinoma scRNA-seq dataset(22) had ~ 3,000 fusion candidates found in at least two cells (excluding candidates involving T cell receptor related genes). Since these T cells are normal cells, true fusions should be very rare in this data set. To control for false discoveries, scFusion independently applies a statistical model and a deep learning model (**Materials and Methods**). Finally, scFusion filters out fusion candidates whose number of supporting discordant reads is ten times more than the supporting split-mapped reads and the candidates with a partner gene involving in more than five fusion candidates.

There are two essential assumptions of the statistical model in scFusion: 1) the candidate fusion list only contains a very small fraction of true fusions, and 2) the true fusion transcripts generally should have more supporting cells/reads than background noises with similar characteristics. The distribution of background noises can be estimated using all candidate fusions. True fusions can be identified by comparing with the background distribution. We

observed that, for each fusion candidate, the number of supporting chimeric reads in a cell depended on the expression of partner genes and local GC content (Figure 2A, B). We describe this dependence using a generalized additive model based on the zero inflated negative binomial (ZINB) distribution. After the model parameters are estimated, we perform a statistical test to test fusion candidates not coming from the background noise and obtain a p-value for each fusion candidate. To effectively control for FDR, we split the candidate fusion list into two subsets, a high-quality fusion candidate subset and a low-quality fusion candidate subset. We use the low-quality subset as the negative control to determine the p-value cutoff for FDR control (**Materials and Methods**).

The statistical model alone is not sufficient to filter out all false fusion candidates since false positive fusion candidates may be induced frequently in single cells during the experimental precedure of cell lysising and sequencing. We therefore developed an independent deep learning model-based method to filter these false positives. This deep learning model assumes that technical chimeric artefacts have unique features, which can be learned and used for distinguishing the technical chimeric artefacts from real fusion events. Here, we formulate the problem as a classification problem and use a bi-directional Long Short Term Memory network (bi-LSTM)(23, 24) to learn the unknown characteristics of technical artefacts. Each single cell usually has over 10,000 chimeric reads (Figure S2A) and the vast majority of them are obviously not signals of gene fusions but technical artefacts. We set the negative training data as the subsequences from chimeric reads, representing the technical artefacts. An ideal positive training data would be chimeric reads from true fusions. Unfortunately, we do not know which chimeric reads are from true fusions. Even if we knew some, the number of such reads would be too small to train the bi-LSTM network. To overcome this challenge, a proxy task strategy is applied: we set the positive training data as sequences generated by concatenating random pairs of short reads. Since the sequences are randomly generated, they should not contain features of technical chimeric reads and hence characteristics of technical artefacts could be learned by comparing with these random sequences. Details of the bi-LSTM is described in the **Materials and Methods** (also see Figure S3A). Using this bi-LSTM model, scFusion gives each fusion candidate a technical artefact score. By default, fusions with scores greater than 0.75 are filtered. The training step is computationally expensive. To expediate the training, scFusion provides a pre-trained model that can be used as the initial value to train bi-LSTM models for new datasets.

We evaluated the performance of the bi-LSTM model using six publicly available scRNA-seq datasets(22, 25-29). The bi-LSTM achieved a median of 0.884 for the area under curve

(AUC) of the receiver operating characteristic (ROC) curve (Figure 2C). The median AUC of the precision-recall (PR) curve (AUPR) was 0.913 (Figure 2D). Note that if we directly used the pre-trained model, the median AUC and AUPR were 0.673 and 0.749 (Figure S3B, C), respectively. Since the bi-LSTM model was not trained using true fusions, true fusions could be filtered by this model. To evaluate this possibility, we applied the bi-LSTM models trained using six public scRNA-seq data to the sequences of 3500 gene fusions reported in Pan-Cancer Analysis of Whole Genomes (PCAWG) studies(30, 31). The PCAWG fusions can be viewed as gold strandard true fusion candidates. The densities of the predicted artefact probabilities of the PCAWG fusions peaked at around 0.1 (Figure 2E). In comparison, the densities of the chimeric reads' score peaked at around 0.95 (Figure 2F). More than 90% of the PCAWG fusions had artefact scores smaller than 0.5, and only ~5% had scores larger than 0.75. These indicated that the bi-LSTM model could effectively filter technical chimeric artefacts at the expense of filtering a very small portion of true fusions. The convolutional neural network (CNN) is another popular neural network model used in many biological applications(32). We also built a CNN model for comparison and found that the bi-LSTM generally performed better than the CNN (Supplementary Material, Figure S4). Hence, we use the bi-LSTM in all following data analyses.

scFusion detects fusions with higher precision in simulation

We first used simulation to evaluate the performance of scFusion and compared with several popular bulk methods including Arriba(18), STAR-Fusion(19), FusionCatcher(12) and EricScript(17). The simulation data was generated using FusionSimulatorToolkit (19). This toolkit can simulate RNA-seq data with gene fusions by learning from a real RNA-Seq dataset such as its expression, insert size, read length and mutation rate. We provided the immune cell scRNA-seq(22) data to FusionSimulatorToolkit to generate RNA-seq data with 150 simulated fusions at various gene expression levels. However, the patterns of technical chimeric reads are unknown. FusionSimulatorToolkit and other available RNA-seq data simulators cannot generate chimeric reads mimicking those in real scRNA-seq data. Observing that immune cells are normal cells, other than chimeric reads generated from recombinations of T Cell Receptor (TCR) genes in T cells and immunoglobulin genes in B cells, almost all other chimeric reads should come from technical artefacts. Thus, we randomly chose chimeric reads not involving TCR and immunoglobulin genes from the immune cell scRNA-seq data and added them to the simulated data. Chimeric reads from one cell's data were only added to simulation data of one cell. This simulation process guaranteed that the chimeric reads in simulation data were similar to those in real scRNA-

seq data and that the simulation faithfully reflected the performance of scFusion in real scRNA-seq data.

We set the percentage of chimeric reads to be 1%, similar to those in the real scRNA-seq data (Figure S2B). To investigate the effect of single cell numbers and sequencing coverages on the fusion detection, we varyed single cell numbers (500 and 1,000 cells) and data sizes of each single cell (2, 3 and 4 million reads, similar to those in real data, see Figure S2C). In total, we had six different simulation setups and we generated ten datasets for each setup. Each simulated fusion was randomly added to 20% cells. For bulk methods, we only considered fusions that were reported in at least two cells to reduce their false positives. Figure 3 and Figure S5 shows the precisions and recalls of these methods. For example, in simulation scenario of 1000 single cells and 3 million reads per cell, the precision and F-socre of scFusion are 0.94 and 0.93, respectively. In comparison, the precisions of the bulk methods are only 0.13-0.70 and the F-scores are 0.23-0.72. Clearly, scFusion has higher, often much higher, precision and F-score than other methods. In comparison, although STAR-Fusion and Arriba found almost all fusions, they detected a large number of false positives. The fusions missed by scFusion are mostly fusions with low expression levels (Figure S6).

scFusion has superior computational efficiency in real scRNA-seq data

We first compared the computational time of different algorithms in real scRNA-seq data(Figure 4). We considered three scRNA-seq data. The three scRNA-seq datasets are a newly sequenced spike-in scRNA-seq data (126 cells), a T cell data (2355 cells) and a multiple myeloma data (597 cells). Details about the data is described below. The computational time of scFusion is only about a half of Arriba and is only ~10% or less of STAR-Fusion, EricScript and FusionCatcher, demonstrating superior computational efficiency than other bulk methods.

scFusion detects fusions with less false discoveries in a single cell spike-in dataset

To test whether scFusion can detect fusions in real scRNA-seq data, we spiked-in 5 known gene fusions to single cells and performed single cell sequencing(8, 9) (**Materials and Methods**). The five added gene fusions were *EML4-ALK*, *CCDC6-RET*, *ERG-TMPRSS2*, *COL1A1-PDGFB* and *GOPC-ROS1* (Figure S7A). In total, we obtained scRNA-seq data of 126 single cells. Based on these cells, scFusion reported 4 out of 5 spike-in gene fusions and 10 other fusions (Table S1, S2). scFusion did not detect *CCDC6-RET* since the fusion

occured in only two cells and did not achieve the significance level. The bulk methods also detected 4 or 5 spike-in fusions (Table S3-6), but they reported much more fusions (60, 2845, 353, and 898 for STAR-Fusion, EricScript, Arriba, and FusionCatcher, respectively), indicating potentially high FDRs. We also performed bulk RNA-seq for the spike-in data and found that 79% (11) of fusions detected by scFusion had 2 or more supporting chimeric reads in the bulk data, suggesting scFusion reported fusions might have high true positive rate. In comparison, only 27% (16), 12% (354), 9% (32) and 28% (249) of fusions detected by STAR-Fusion, EricScript, Arriba, and FusionCatcher had supporting chimeric reads in the bulk data, respectively (Figure S7B).

scFusion demonstrates high sensitivity in detecting marker fusions in a T cell dataset

The T cell data consists of 2,355 T cells from the immune data containing ~7,000 immune cells profiled from patients with liver cancer (22). T cells of this data are non-malignant cells. Other than the V(D)J recombinations of TCR genes, gene fusions should be very rare in T cells. scFusion, Arriba, STAR-Fusion, FusionCatcher and EricScript identified 8, 574, 87, 716 and 4,306 gene fusions, respectively (Figure 5A, Table S7-11). Among the fusions detected by scFusion, 6 involve TCR genes and 4 out of 8 (50%) are V(D)J recombinations, indicating that many of these candidates are likely true positives. In comparison, only 1.1% (1) of STAR-Fusion candidates are V(D)J recombinations and no candidate of other bulk methods are V(D)J recombinations (Figure 5B). The two most significant V(D)J recombinations given by scFusion are *TRAJ33-TRAV1-2* and *TRAJ12-TRAV1-2*, with 128 and 21 supporting cells, respectively. Mucosal-associated invariant T (MAIT) cells are known to express the invariant *TRAJ33-TRAV1-2* and *TRAJ12-TRAV1-2* TCR α-chain (22, 33). Thus, the single cells with one of these fusions are likely MAIT cells. *SLC4A10* is often used as a marker gene of MAIT cells (34). *SLC4A10* is indeed only expressed in a cluster of T cells and many of these T cells had the *TRAJ33-TRAV1-2* or *TRAJ12-TRAV1-2* fusion (Figure 5C, D). Differential expression analysis between the cells with and without these recombinations identifies 70 upregulated genes in the cells with the recombinations, among which *TRAJ33, TRAV1-2* and *SLC4A10* are the top three most significantly upregulated genes (Figure S8A, B). Further, the *SLC4A10* expression are highly significantly associated with the fusion (Fisher's exact test, P-value < 10^{-16}; Table 1). These results indicate that the *TRAJ33-TRAV1-2* and *TRAJ12-TRAV1-2* fusions identified by scFusion are *bona fide* fusions and the cells with either fusion are MAIT cells. MAIT cells are an important component of the immune system. However, until recently, the detection of MAIT cells still relies on the combinations of cell markers and it is unclear how well these markers define the MAIT cells in different tissues or diseases(35). scFusion provides an alternative way to

sensitively define the MAIT cells. STAR-Fusion was the only bulk method that identified the *TRAJ33-TRAV1-2* fusion (62 cells) (Figure 5E), and no bulk method reported any cells having the *TRAJ12-TRAV1-2* fusion (Figure 5F), indicating that scFusion is more powerful in detecting shared fusions among single cells.

Senstitive fusion detection by scFusion provides mechanistic insights in a multiple myeloma dataset

Finally, we applied scFusion to a multiple myeloma (MM) dataset consisting of 597 MM single cells from 15 patients (28). MM is a cancer of plasma cells. Approximately half of the myelomas have immunoglobulin heavy (*IgH*) chain translocations and around 10% of the myelomas have translocations involving immunoglobulin lambda (*IgL*) light chain locus (36, 37). In this dataset, scFusion, Arriba, STAR-Fusion, FusionCatcher and EricScript identified 44, 378, 149, 167 and 2,162 gene fusions, respectively (Figure 6A, Table S12-16). Around 88.6% (39) of scFusion candidates involve immunoglobulin genes (including 33 recombinations of immunoglobin genes), much higher than that of bulk methods. (TableS12, Figure 6B). scFusion successfully identified the recurrent *IgH-WHSC1* fusion in MM with two different breakpoints at *WHSC1*, 1902353 and 1905943 at chromosome 4 (Table S12). The *IgH-WHSC1* fusions are in-frame fusions of *WHSC1*. All 52 cells with the breakpoint at 1902353 are from the patient SMM0. Similarly, all 20 cells with the other breakpoint are from the patient RRMM2 (Figure 6C). The expression of *WHSC1* is significantly higher in cells with the *WHSC1* fusions than other cells (Figure 6D). Interestingly, in cells with the *WHSC1* fusions, the sequencing coverage of *WHSC1* sharply increases at the downstream of the breakpoints, but the sequencing coverage of *WHSC1* in other cells largely keeps constant, indicating that the fusions probably lead to the over-expression of *WHSC1* (Figure 6E, Figure S8D). *WHSC1*, also known as *NSD2*, is one of the most commonly fused genes with IgH in multiple myeloma(38-40). *WHSC1* is a known oncogene listed in COSMIC (41). Overexpression of *WHSC1* drives the chromatin change in an H3K36me2-dependent manner(42). Differential expression analysis found 115 upregulated genes and 12 down-regulated genes in the cells with the *IgH-WHSC1* fusions (q-value < 0.05 and log2 fold change < -0.5 or > 0.5) (Figure S8C, Table S17). The upregulated genes include genes known be co-expressed with *WHSC1* such as *MAL* (43) and *SCARNA22* (44). The downregulated genes include known oncogenes in MM such as *CCND1* and *FRZB*. In fact, *CCND1* and *FRZB* tend to only express in cells without the *IgH-WHSC1* fusions (Figure S8E, F). The bulk methods also detected the *IgH-WHSC1* fusions, but they reported less number of cells with the fusions than scFusion (Figure 6F) and potentially much more false positives (Figure 6A,B). The large number of false positives given by the bulk methods makes it very

difficult for downstream analysis, thus limiting their application in single cell analyses. In comparion, scFusion has much fewer false discoveries and is more powerful in detecting important shared fusions such as *IgH-WHSC1*.

Discussion

We describe a single cell gene fusion detection method scFusion by integrating fusion signals from multiple cells. The major challenge of fusion detection in single cells is the large number of false positives. To address this challenge, we introduced a statistical testing procedure to control the FDR. This procedure assumes most of fusion signals are technical noises and true fusions generally have stronger signal than technical noises. In addition, some systematic technical artefacts can occur recurrently in multiple single cells and might be assigned with a significant p-value by the statistical procedure. We developed a deep learning model to learn the unknown technical artefacts and to filter the false postives generated by these artefacts.

We evaluated the performance of scFusion using simulation data and three real scRNA-seq datasets. In the simulation, a critical problem is to generate technical chimeric artefacts. Unfortunately, the mechanisms generating these artefacts are largely unknown and it is difficult to generate chimeric artefacts that have the same pattern as those in the real scRNA-seq data. We bypassed this problem by taking chimeric reads from real scRNA-seq data and adding them to the simulation data. In this way, we guaranteed that the simulation faithfully reflects the performance of fusion detection methods in real data. scFusion outperformed the bulk methods in terms of precision and F-score. In the real data analysis, we found that scFusion generally detected much less fusions compared with the bulk methods. Especially, scFusion only detected 8 fusions in the T cell data while the bulk methods detected much more fusions. Considering that the T cells are normal cells, they should not have many fusions, implying that many fusions detected by the bulk methods are false positives.

We demonstrated application of scFusion in two different scRNA-seq datasets. In both datasets, scFusion was able to identify subgroups of single cells with specific gene fusions, i.e. the MAIT cells with the invariant TCR recombinations and the MM cells with the *IgH-WHSC1* fusions. MAIT cells in human are known to express three TCR α-chains, of which the most abundant is *TRAJ33-TRAV1-2 (35).* scFusion identified two of the three and found

that *TRAJ33-TRAV1-2* about 5 times more abundant than *TRAJ12-TRAV1-2*. The *TRAJ20-TRAV1-2* was not identified possibly because it was rare in MAIT cells. Gene differential expression analysis discovered 15 genes significantly differentially expressed between *TRAJ33-TRAV1-2* and *TRAJ12-TRAV1-2* cells (Table S18). As expected, the expressions of *TRAJ33* and *TRAJ12* are higher in *TRAJ33-TRAV1-2* and *TRAJ12-TRAV1-2* cells, respectively. Interestingly, *ALPK1* and *TIFA* are highly expressed in the cells with *TRAJ12-TRAV1-2* (Figure S9). Recent studies(45) show that *ALPK1-TIFA* axis is a core innate immune pathway against patheogens such as *Helicobactor pylori*, implying that MAIT cells expressing different TCR α-chains might have different roles in the immune system. In the MM data, the *IgH-WHSC1* fusions are the most significant immunoglobulin-related fusions reported by scFusion, leading to the overexpression of *WHSC1*. *WHSC1* plays an important role in cell development. Overactivating *WHSC1* promotes the uncontrolled growth and division of cancer cells (46). In the MM data, *WHSC1* is highly expressed in single cells from three patients (SMM0, RRMM1 and RRMM2). scFusion did not find *WHSC1* fusions in singles cells from RRMM2. It is likely that the expression of WHSC1 was activated in RRMM2 by mechnisms other than *WHSC1* fusions or that the fusion was missed by scFusion. Taken together, these applications show that accurate gene fusion detection at single cell level could provide key information for defining cellular subtypes or subclones, which might have important implications for many applications, such as identifying drug resistant or sensitive subclones in tumor.

scRNA-seq technologies based on the unique molecular identifier (UMI) such as 10X Genomics(47) and Drop-seq(48) are more cost-effective and more widely used than full-length scRNA-seq technologies. However, the UMI-based methods only sequence RNA 3' ends and only allow detecting fusions whose breakpoints are close to the 3' ends of the fusion RNAs. scFusion may also be applied to these UMI-based scRNA-seq data, but its detection power will be limited. Another potential limitation of scFusion is that the deep learning model inevitably filters a small portion of true fusions. At the cutoff 0.75, the deep learning model filters ~ 5% of the PCAWG fusions. The percentage of falsely filtered fusions by the deep learning model is possibly less than this number since the PCAWG fusions may also have false positives. On the other hand, since the cutoff is conservative, a large portion of technical artefacts will not be filtered. This problem may be ameliorated by building a more accurate deep learning classifier. For example, after we have more true fusions, we can build a model using the sequences from the true fusion as the negative set and thus reduce the possibility of incorrectly filtering of true fusions.

Gene fusions are one of the most widely studied biological events in cancer. Analysis of gene fusions at single cell level will provide unprecedent opportunities to study their roles in tumor development, tumor heterogeneity as well as tumor cell's responses to various pharmatheutical therapies. We expect that scFusion will find its application in many different single cell researches.

Data Availability

Raw data of the spike-in data will be available at the Genome Sequence Archive (GSA) of BIG Data Center (http://bigd.big.ac.cn/gsa), Beijing Institute of Genomics (BIG), Chinese Academy of Sciences, with an accession number HRA000343. The scRNA-seq data GSE81812, GSE99795, GSE110499, GSE118900, GSE127298, GSE140228 were obtained from the Gene Expression Omnibus (GEO) (https://www.ncbi.nlm.nih.gov/geo/).

Software Availability

scFusion is available at github (https://github.com/XiDsLab/scFusion).

Acknowledgements

This work was supported by the National Natural Science Foundation of China [11971039, 11471022 and 71532001] and the Recruitment Program of Global Youth Experts of China.

Materials and Methods

Statistical Model

Let y_{ij} be the number of split-mapped reads supporting a fusion candidate *i* in a cell *j*. Denote Y_{ij} the random variable corresponding to y_{ij}. Theoretically, the random variable Y_{ij} should follow a mixture distribution. One component of the mixture distribution is the distribution of supporting reads of true gene fusions and another is the distribution of supporting reads of the technical chimeric artefacts. However, since the candidate fusions have very few true fusions, we can safely use all y_{ij} to estimate the distribution of split-mapped reads from technical chimeric artefacts. With the estimation of this background distribution, we can then perform statistical tests to identify candidates that are unlikely to be generated from the background distribution. We assume that Y_{ij} follows a zero-inflated negative binomial (ZINB) distribution(49). The ZINB distribution has three parameters. One parameter is p_i, the probability that the cell *j* has no split-mapped read supporting the fusion candidate *i* or $p_i = P(Y_{ij} = 0)$. The other two parameters of the ZINB are the mean μ_{ij} and the overdispersion parameter λ of the negative binomial (NB) distribution. Thus, we have $Y_{ij} \sim ZINB(p_i, \mu_{ij}, \lambda)$. Conditional on $Y_{ij} > 0$, Y_{ij} follows a zero-truncated NB distribution. The

ZINB distribution could depend on other factors, such as the expression levels of the partner genes and the GC content (50). Analysis of several different scRNA-seq data shows that the number of technical chimeric artefacts indeed strongly depends on the gene expression and the GC content (Figure 2A, B). Let $EL_{ij} < EH_{ij}$ be the expressions of the two partner genes corresponding to Y_{ij} and GC_i be the GC content of the exonic sequence near the junction of the candidate gene (200bp). Further, define $\overline{EL_i} < \overline{EH_i}$ as the mean expression of the two partner genes of the candidate fusion i across all single cells. We consider the following model

$$\mathrm{logit}(p_i) = \beta_{10} + f(GC_i) + \beta_{11}\overline{EL_i} + \beta_{12}\overline{EH_i},$$
$$\log(\mu_{ij}) = \beta_{20} + g(GC_i) + \beta_{21}EL_{ij} + \beta_{22}EH_{ij},$$

where f and g are unknown functions, and the $\boldsymbol{\beta}_1 = (\beta_{10}, \beta_{11}, \beta_{12})$ and $\boldsymbol{\beta}_2 = (\beta_{20}, \beta_{21}, \beta_{22})$ are unknown parameters. We represent f and g using spline functions, $f(x) = \sum_{k=1}^{K} \beta_{kf} B_k(x)$ and $g(x) = \sum_{k=1}^{K} \beta_{kg} B_k(x)$, where K is the number of spline base functions (by default K is set as 5). Denote $\boldsymbol{\theta} = (\boldsymbol{\beta}_1, \boldsymbol{\beta}_2, \boldsymbol{\beta}_f, \boldsymbol{\beta}_g)$ with $\boldsymbol{\beta}_f = (\beta_{1f}, \cdots \beta_{Kf})$ and $\boldsymbol{\beta}_g = (\beta_{1g}, \cdots \beta_{Kg})$. We estimate the unknown parameters $\boldsymbol{\theta}$ by maximizing the following likelihood,

$$l(\beta_1,\ \beta_2, \lambda) = \prod_{i=1}^{N} l_i\left(\boldsymbol{\theta} \middle| \sum_{j=1}^{n} 1_{y_{ij}>0} \geq 2\right),$$

$$l_i\left(\boldsymbol{\theta} \middle| \sum_{j=1}^{n} 1_{y_{ij}>0} \geq 2\right) = \frac{p_i^{\sum_{j=1}^{n} 1_{y_{ij}=0}} \prod_{j:y_{ij}>0} \frac{\phi(y_{ij}; \mu_{ij}, \lambda)}{1 - \phi(0; \mu_{ij}, \lambda)}}{1 - p_i^n - n(1-p_i)p_i^{n-1}},$$

where N is the number of fusion candidates supported by at least 2 cells, n is the number of cells, ϕ is the probability density function of NB distribution with mean μ_{ij} and overdispersion λ. Note that to reduce computational burden, we only consider the candidates with at least two cells having supporting split-mapped reads and thus the likelihood l_i for the candidate i is a conditional probability.

Statistical Test for Significant Fusions

After estimating the unknown functions and unknown parameters, we have the parameter estimates $\hat{p}_i, \hat{\mu}_{ij}$ and $\hat{\lambda}$. We use these estimates and a resampling scheme to obtain a p-value for each fusion candidate. Specifically, for each fusion candidate i, we sample $\tilde{Y}_{ij}^{(b)}$ from $ZINB(\hat{p}_i, \hat{\mu}_{ij}, \hat{\lambda})$ for each cell j and obtain the sum $\tilde{S}_i^{(b)} = \sum_{j=1}^{n} \tilde{Y}_{ij}^{(b)}$ $(b = 1, \cdots, B)$. Denote $\tilde{v}_i$ and $\tilde{\sigma}_i^2$ be the sample mean and variance of $\tilde{S}_i^{(b)}$, respectively. The distribution of

$\tilde{S}_i^{(b)}$ can be approximated by a normal distribution with the mean and variance approximately $\tilde{v}_i$ and $\tilde{\sigma}_i^2$, respectively. Let $S_i = \sum_{j=1}^{n} Y_{ij}$. The p-value for the fusion candidate i is set as $p_i = 1 - \Phi((S_i - \tilde{v}_i)/\tilde{\sigma}_i)$, where Φ is the cumulative distribution of the standard normal distribution. We set $B = 1{,}000$ in all analyses. To determine a p-value cutoff to control the FDR, we split our candidate fusion set to two subsets. The first subset is a high-quality subset which more likely contains the true gene fusions and the second subset is the remaining candidates. Suppose that n_1 and n_2 as the total number of candidates in the first and the second subset, respectively. Given a p-value cut-off c, let $m_1(c)$ and m_2(c) be the number of candidates in the two subsets with p-values less c, respectively. Since the second subset contains much fewer true positives than the first subset, $(n_1 + n_2)\frac{m_2(c)}{n_2}$ can be used as an estimate of total number of false discoveries at the p-value cutoff c and thus the FDR is roughly $fdr(c) = \frac{m_2(c)}{n_2}\frac{n_1+n_2}{m_1(c)+m_2(c)}$. We choose c such that $fdr(c) \leq \alpha$ for a given α (usually 0.05). In generally, we believe that candidates with more supporting cells are more likely to be true. Hence, we choose the first subset as the fusion candidates with at least 1% of the total cells having the fusion and with at least s supporting reads per cell on average, where s is taken as 1.25 in all simulation and real data analysis.

The bi-LSTM

The negative training data of the bi-LSTM is chosen as the subsequences (60 bp) of chimeric reads covering the junction positions and the junction positions are required to be at 15-45 bp of the subsequences. The positive training data is the similar 60bp subsequences of randomly concatenated short read pairs. In the bi-LSTM (Figure S3A), the DNA sequences, with 60 nucleotides and one fusion site, are given as the input to the embedding layer. The four types of nucleotide (i.e., A, T, G and C) and the fusion site are represented by five different 5-dimensional feature vectors. The output of the embedding layer is passed on to three sequence-to-sequence bi-LSTM layers (with 32, 64, and 128 bi-LSTM units, respectively) and further to a sequence-to-one bi-LSTM layer for sequential feature extraction. The extracted features are fed to two fully connected layers and finally to a softmax layer to produce the softmax probabilities of the read being classified to technical chimeric artefacts. In the training process, the binary cross-entropy is used as the loss function and model parameters are updated using the Adam optimizer(51). The model is pre-trained for 200 epochs with batch size set to 500. The retraining is trained for 30 epochs with the pre-trained model as initial value.

Gene fusion spike-in and single cell sequencing

Five fusion genes cDNA sequences were synthesized and constructed into lentiviral vectors respectively. To construct a cell line with stable expression of fusion genes, every lentiviral vector and two auxiliary packaging plasmids were co-transfected into the 293T cells. After 48 hours, the supernatant was collected from the 293T cells and filtered through a 0.45 uM membrane. The five different recombinant lentiviral particles containing the target fusion genes and the green fluorescent protein (GFP) reporter gene were collected. Then, the five recombinant lentivirus particles infected into 293T cells, respectively. 72 hours after infection, the medium was changed and the expression of GFP in cells was checked under a fluorescence microscope for determining if lentivirus infection was successful. After the infection, five cell lines expressing the target fusion genes were collected. The single GFP positive cells were filtered into a 96-well PCR plate by fluorescence activated cell sorting (FACS) for the single-cell RNA library construction. Poly(A)-transcripts of total RNA of single cells were reverse transcribed and amplified using the SMART-seq2 (8, 9) protocol. The amplified cDNA was tagmented by Nextera XT kit (Illumina) and libraries were sequenced by NovaSeq (Illumina). The 293T cells were purchased from the National Infrastructure of Cell Line Resource (http://www.cellresource.cn/).

scRNA-seq data analysis

For scFusion, short reads are first aligned with STAR(v 2.7.4a) to the human reference genome (hg19). scFusion only considers short reads mapped to uniquely mappable positions in the exonic regions of the reference genome (uniquely mappable for 75bp sequences). Then, the split-mapped reads are clustered. If the breakpoints of two split-mapped reads are no larger than 3 bp away from each other, the two split-mapped reads are clustered together. A fusion candidate's breakpoint is taken as the median of the breakpoint positions of its all supporing chimeric reads.

Arriba(v1.0.1), EricScript(v0.5.5b), STAR-Fusion(v1.8.1), FusionCatcher(v1.10) were all runned on the default parameters. The reference genome was always chosen as hg19. For the bulk methods, we also applied the same *ad hoc* filters of scFusion to make different algorithms comparable. Specifically, we applied the pseudogene-, lncRNA-, no-approved-symbol-gene-, intron-, too-many-partner- and too-many-discordant- filters to the fusion candidates of bulk methods.

Gene expression analysis

The expression matrix of T cell and multiple myeloma dataset were downloaded from the Gene Expression Omnibus (GEO) (https://www.ncbi.nlm.nih.gov/geo/). First, we used Seurat

(v 3.2.0) (52, 53) to read the Transcripts Per Million (TPM) matrix. The expression was further normalized using the NormalizeData function in Seurat. The highly variable genes were identified using the function FindVariableGenes. Their expression was scaled and centered along each gene using ScaleData. Then we performed dimension reduction using principal component (PC) analysis. We selected the first 30 PCs for t-distributed stochastic neighbor embedding (tSNE), and tSNE plots were generated using Seurat. To identify differentially expressed genes, we used the function FindAllMarkers in Seurat with the Wilcoxon rank sum test. Genes expressed in at least 10% cells within the cluster and with the log fold change more than 0.5 and the adjusted p-value smaller than 0.05 were considered as differentially expressed genes.

Supplementary Text

The convolutional neural network model

The convolutional neural network (CNN) model is mainly composed of three layers: a convolution layer, a pooling layer and a fully connected layer (Figure S4A). The input of the network is a 60bp read, which contains the bases near the breakpoint of the fusion gene, and an integer between 15 and 45 that indicates the position of the breakpoint. The output is a probability that the sequence is a technical chimeric artefact.

We first convert the input sequence to a padded 5-row array that each row represents one of four bases (A, G, T, C) or the breakpoint position. Specifically, given the size of convolution kernel m, we convert a sequence S of length n to a 5*(n+2m-2) array A in this way:

$$A_{i,j} = \begin{cases} 0.25 & if\ \ i = 1 \ldots 4\ and\ j < m\ or\ j > n - m \\ 1 & if\ (i, S_{j-m+1}) = (1, A)\ or\ (2, G)\ or\ (3, C)\ or\ (4, T) \\ 1 & if\ i = 5\ and\ the\ breakpoint\ position\ is\ j - m + 1 \\ 0 & otherwise \end{cases}$$

where $A_{i,j}$ denotes the (i, j) element of A and S_i denotes the i-th base of S.

The convolutional layer takes the array as input, and each convolution kernel performs one-dimensional convolution on this 5-channel input. The number of kernels as well as its size are tunable parameters. In our model, we use 2048 convolution kernels of length 16 ($m = 16$) by default. Therefore, the output of this layer is of size 2048*75. The output feature map of each kernel is then rectified by adding a bias and being activated by ReLU.

The pooling layer performs max operation on the rectified features, aiming to integrate the features obtained by the convolution. After this stage, we get a 2048-dimensional vector.

Finally, the feature vector is passed to the fully connected layer, which consists of a hidden layer and an output layer. The hidden layer is of 256 neurons by default and the output layer is a single neuron with Sigmoid function.

We use negative log-likelihood as the loss function, and Adam(51) with L2 regularization for optimization. We use mini-batch to speed up training and add a dropout layer after convolution to reduce overfitting. By default, batch size, learning rate, weight decay and dropout rate is set to 512, $3*10^{-3}$, $1*10^{-4}$ and 0.25 respectively.

Commands

We list how we use the bulk method in the following.

STAR mapping:

STAR --runThreadN 20 --genomeDir CTAT_GENOME_LIB/GRCh37_ gencode_v19_CTAT_lib_Feb092018/ctat_genome_lib_ build_dir/ref_genome.fa.star.idx --readFilesIn /1_1.fastq 1_2.fastq --outSAMtype BAM SortedByCoordinate --chimOutType SeparateSAMold --outSAMunmapped Within KeepPairs --quantMode GeneCounts --outFileNamePrefix 1/human --chimSegmentMin 12 --chimJunctionOverhangMin 12 --alignSJDBoverhangMin 10 --alignMatesGapMax 100000 --alignIntronMax 100000 --chimSegmentReadGapMax 3 --alignSJstitchMismatchNmax 5 -1 5 5

STAR-Fusion:

STAR-Fusion-v1.8.1/STAR-Fusion --left_fq 1_1.fastq --right_fq 1_2.fastq --genome_lib_dir /GRCh37_gencode_v19_CTAT_lib_Oct012019.plug-n-play/ctat_genome_lib_build_dir/ --CPU 20 --output_dir STAR_Fusion_Res/

EricScript:

Ericscript/ericscript.pl -db Ericscript/ericscript_db_homosapiens_ensembl73 -p 20 -name 1 -o EricRes/1 1_1.fastq 1_2.fastq

Arriba:

Arriba is piped with STAR:

STAR --runThreadN 20 --genomeDir CTAT_GENOME_LIB/GRCh37_ gencode_v19_CTAT_lib_Feb092018/ctat_genome_lib_ build_dir/ref_genome.fa.star.idx --genomeLoad NoSharedMemory --readFilesIn 1_1.fastq 1_2.fastq --outStd BAM_Unsorted --outFileNamePrefix OUTDIR --outSAMtype BAM Unsorted --outSAMunmapped Within --outBAMcompression 0 --outFilterMultimapNmax 1 --outFilterMismatchNmax 3 --

chimSegmentMin 10 --chimOutType WithinBAM SoftClip --chimJunctionOverhangMin 10 --chimScoreMin 1 --chimScoreDropMax 30 --chimScoreJunctionNonGTAG 0 --chimScoreSeparation 1 --alignSJstitchMismatchNmax 5 -1 5 5 --chimSegmentReadGapMax 3 | arriba -x /dev/stdin -o OUTDIR/fusions.tsv -O OUTDIR/fusions.discarded.tsv -a "$ASSEMBLY_FA" -g "$ANNOTATION_GTF" -b "$BLACKLIST_TSV" -T -P

FusionCatcher:

FusionCatcher/bin/fusioncatcher -d FusionCatcher/data/human_v95 -i 1 1.fastq,1_2.fastq -o FusionCatcherRes

Reference

1. J. D. Rowley, Identificaton of a translocation with quinacrine fluorescence in a patient with acute leukemia. *Annales de Genetique* **16**, 109-112 (1973).
2. P. C. Nowell, D. A. Hungerford, Chromosome studies on normal and leukemic human leukocytes. *Journal of the National Cancer Institute* **25**, 85-109 (1960).
3. F. Demichelis *et al.*, TMPRSS2:ERG gene fusion associated with lethal prostate cancer in a watchful waiting cohort. *Oncogene* **26**, 4596-4599 (2007).
4. Y. L. Choi *et al.*, EML4-ALK mutations in lung cancer that confer resistance to ALK inhibitors. *New England Journal of Medicine* **363**, 1734-1739 (2010).
5. T. O'Hare *et al.*, In vitro activity of Bcr-Abl inhibitors AMN107 and BMS-354825 against clinically relevant imatinib-resistant Abl kinase domain mutants. *Cancer Research* **65**, 4500-4505 (2005).
6. A. T. Shaw *et al.*, Crizotinib versus chemotherapy in advanced ALK-positive lung cancer. *New England Journal of Medicine* **368**, 2385-2394 (2013).
7. T. W. Laetsch *et al.*, Larotrectinib for paediatric solid tumours harbouring NTRK gene fusions: phase 1 results from a multicentre, open-label, phase 1/2 study. *The Lancet Oncology* **19**, 705-714 (2018).
8. S. Picelli *et al.*, Smart-seq2 for sensitive full-length transcriptome profiling in single cells. *Nature Methods* **10**, 1096-1098 (2013).
9. S. Picelli *et al.*, Full-length RNA-seq from single cells using Smart-seq2. *Nature protocols* **9**, 171-181 (2014).

10. D. Ramskold *et al.*, Full-length mRNA-Seq from single-cell levels of RNA and individual circulating tumor cells. *Nature Biotechnology* **30**, 777-782 (2012).
11. K. Chen *et al.*, BreakFusion: targeted assembly-based identification of gene fusions in whole transcriptome paired-end sequencing data. *Bioinformatics* **28**, 1923-1924 (2012).
12. D. Nicorici *et al.*, FusionCatcher - a tool for finding somatic fusion genes in paired-end RNA-sequencing data. *BioRxiv*, 011650 (2014).
13. N. M. Davidson, I. J. Majewski, A. Oshlack, JAFFA: High sensitivity transcriptome-focused fusion gene detection. *Genome Medicine* **7**, 43 (2015).
14. R. W. Francis *et al.*, FusionFinder: a software tool to identify expressed gene fusion candidates from RNA-Seq data. *PLoS ONE* **7**, e39987 (2012).
15. Y. Li, J. Chien, D. I. Smith, J. Ma, FusionHunter: identifying fusion transcripts in cancer using paired-end RNA-seq. *Bioinformatics* **27**, 1708-1710 (2011).
16. A. McPherson *et al.*, deFuse: an algorithm for gene fusion discovery in tumor RNA-Seq data. *PLoS Computational Biology* **7**, e1001138 (2011).
17. M. Benelli *et al.*, Discovering chimeric transcripts in paired-end RNA-seq data by using EricScript. *Bioinformatics* **28**, 3232-3239 (2012).
18. S. Uhrig. Arriba: Fast and accurate gene fusion detection from RNA-Seq data. https://github.com/suhrig/arriba.
19. B. J. Haas *et al.*, Accuracy assessment of fusion transcript detection via read-mapping and de novo fusion transcript assembly-based methods. *Genome Biology* **20**, 213 (2019).
20. A. Dobin *et al.*, STAR: ultrafast universal RNA-seq aligner. *Bioinformatics* **29**, 15-21 (2013).
21. J. L. Ashurst *et al.*, The Vertebrate Genome Annotation (Vega) database. *Nucleic Acids Research* **33**, D459-D465 (2005).
22. Q. Zhang *et al.*, Landscape and Dynamics of Single Immune Cells in Hepatocellular Carcinoma. *Cell* **179**, 829-845.e820 (2019).
23. M. Schuster, K. K. Paliwal, Bidirectional recurrent neural networks. *IEEE Transactions on Signal Processing* **45**, 2673-2681 (1997).
24. D. Quang, X. Xie, DanQ: a hybrid convolutional and recurrent deep neural network for quantifying the function of DNA sequences. *Nucleic Acids Research* **44**, e107-e107 (2016).

25. L. Yang *et al.*, Single-cell RNA-seq of esophageal squamous cell carcinoma cell line with fractionated irradiation reveals radioresistant gene expression patterns. *BMC Genomics* **20**, 611 (2019).
26. A. M. Horning *et al.*, Single-Cell RNA-seq reveals a subpopulation of prostate cancer cells with enhanced cell-Cycle–Related transcription and attenuated androgen response. *Cancer Research* **78**, 853-864 (2018).
27. J. Fan *et al.*, Linking transcriptional and genetic tumor heterogeneity through allele analysis of single-cell RNA-seq data. *Genome Research* **28**, 1217-1227 (2018).
28. J. S. Jang *et al.*, Molecular signatures of multiple myeloma progression through single cell RNA-Seq. *Blood Cancer Journal* **9**, 2 (2019).
29. A. V. Krivtsov *et al.*, A menin-MLL inhibitor induces specific chromatin changes and eradicates disease in models of MLL-rearranged leukemia. *Cancer Cell* **36**, 660-673. e611 (2019).
30. C. Calabrese *et al.*, Genomic basis for RNA alterations in cancer. *Nature* **578**, 129-136 (2020).
31. P. J. Campbell *et al.*, Pan-cancer analysis of whole genomes. *Nature* **578**, 82-93 (2020).
32. B. Alipanahi, A. Delong, M. T. Weirauch, B. J. Frey, Predicting the sequence specificities of DNA- and RNA-binding proteins by deep learning. *Nature Biotechnology* **33**, 831-838 (2015).
33. C. Zheng *et al.*, Landscape of Infiltrating T Cells in Liver Cancer Revealed by Single-Cell Sequencing. *Cell* **169**, 1342-1356 e1316 (2017).
34. P. T. Rudak, T. Yao, C. D. Richardson, S. Haeryfar, Measles Virus Infects and Programs MAIT Cells for Apoptosis. *The Journal of Infectious Diseases* (2020).
35. D. I. Godfrey, H.-F. Koay, J. McCluskey, N. A. Gherardin, The biology and functional importance of MAIT cells. *Nature Immunology* **20**, 1110-1128 (2019).
36. B. G. Barwick *et al.*, Multiple myeloma immunoglobulin lambda translocations portend poor prognosis. *Nature Communications* **10**, 1911 (2019).
37. P. L. Bergsagel *et al.*, Promiscuous translocations into immunoglobulin heavy chain switch regions in multiple myeloma. *Proceedings of the National*

Academy of Sciences of the United States of America **93**, 13931-13936 (1996).

38. I. Stec *et al.*, WHSC1, a 90 kb SET domain-containing gene, expressed in early development and homologous to a Drosophila dysmorphy gene maps in the Wolf-Hirschhorn syndrome critical region and is fused to IgH in t (1; 14) multiple myeloma. *Human Molecular Genetics* **7**, 1071-1082 (1998).
39. M. Santra, F. Zhan, E. Tian, B. Barlogie, J. Shaughnessy Jr, A subset of multiple myeloma harboring the t (4; 14)(p16; q32) translocation lacks FGFR3 expression but maintains an IGH/MMSET fusion transcript. *Blood, The Journal of the American Society of Hematology* **101**, 2374-2376 (2003).
40. U. Malgeri *et al.*, Detection of t (4; 14)(p16. 3; q32) chromosomal translocation in multiple myeloma by reverse transcription-polymerase chain reaction analysis of IGH-MMSET fusion transcripts. *Cancer Research* **60**, 4058-4061 (2000).
41. S. A. Forbes *et al.*, COSMIC: exploring the world's knowledge of somatic mutations in human cancer. *Nucleic Acids Research* **43**, D805-D811 (2015).
42. A. J. Kuo *et al.*, NSD2 links dimethylation of histone H3 at lysine 36 to oncogenic programming. *Molecular Cell* **44**, 609-620 (2011).
43. J. J. Keats, T. Reiman, A. R. Belch, L. M. Pilarski, Ten years and counting: so what do we know about t(4;14)(p16;q32) multiple myeloma. *Leukemia & Lymphoma* **47**, 2289-2300 (2006).
44. N. Mahajan, J. D. Weber, L. B. Maggi, M. H. Tomasson, ACA11, a Small Nucleolar RNA Activated in Multiple Myeloma, Stimulates Proliferation by Inactivating NRF2 and Increasing Redox Signaling. *The FASEB Journal* **30**, 1054.1057-1054.1057 (2016).
45. S. Zimmermann *et al.*, ALPK1- and TIFA-Dependent Innate Immune Response Triggered by the Helicobacter pylori Type IV Secretion System. *Cell Reports* **20**, 2384-2395 (2017).
46. J. J. Keats *et al.*, Overexpression of transcripts originating from the MMSET locus characterizes all t(4;14)(p16;q32)-positive multiple myeloma patients. *Blood* **105**, 4060-4069 (2005).
47. G. X. Y. Zheng *et al.*, Massively parallel digital transcriptional profiling of single cells. *Nature Communications* **8**, 14049 (2017).

48. E. Z. Macosko *et al.*, Highly Parallel Genome-wide Expression Profiling of Individual Cells Using Nanoliter Droplets. *Cell* 161, 1202-1214 (2015).
49. D. Risso, F. Perraudeau, S. Gribkova, S. Dudoit, J. P. Vert, A general and flexible method for signal extraction from single-cell RNA-seq data. *Nature Communications* 9, 284 (2018).
50. D. Sims, I. Sudbery, N. E. Ilott, A. Heger, C. P. Ponting, Sequencing depth and coverage: key considerations in genomic analyses. *Nature Reviews Genetics* 15, 121-132 (2014).
51. D. P. Kingma, J. Ba, Adam: A method for stochastic optimization. *arXiv preprint arXiv:1412.6980* (2014).
52. A. Butler, P. Hoffman, P. Smibert, E. Papalexi, R. Satija, Integrating single-cell transcriptomic data across different conditions, technologies, and species. *Nature Biotechnology* 36, 411-420 (2018).
53. T. Stuart *et al.*, Comprehensive Integration of Single-Cell Data. *Cell* 177, 1888-1902.e1821 (2019).

Figures and Tables

Figure 1. Overview of scFusion for single cell gene fusion detection. The single cell RNA-seq reads are mapped and supporting reads are identified and clustered to obtain the fusion candidates list. Given the candidate information, a ZINB-based statistical model and a deep learning model are trained to filter the potential false positives.

Figure 2. Features of technical chimeric reads. The number of supporting chimeric reads depends on (**A**) the expression of partner genes and (**B**) the local GC content. The Pearson's Correlations between the number of chimeric reads and the gene expression and the p-values are shown in the figure. The GC content is calculated using sequences near breakpoints (200 bp). (**C**) The ROCs of the bi-LSTM model for different single cell data sets (validation data). The AUCs are also shown. (**D**) The PR curves and their AUPRs. (**E**) The densities of the technical artefact score of gene fusions in the PCAWG study by the bi-LSTM models retrained using six different datasets. (**F**) The densities of the predicted probabilities of chimeric reads. The models are retrained using different datasets.

Figure 3. The precisions and recalls of scFusion and four bulk methods in six different simulation setups. The figures in the two rows correspond to simulations with 500 cells and

1000 cells, and the figures in the three columns correspond to simulations with 2 million, 3 million and 4 million reads in each data. The dots in the figures are the means of precisions and recalls of ten simulations in each setup. The dashed lines are the contour lines with constant F-scores (F-scores are marked in the top-left figure).

Figure 4. The computational time of the five methods for fusion detection in the three scRNA-seq data. The y-axis is the total CPU hours of each method.

Figure 5. The T cell scRNA-seq data. (**A**) The number of detected gene fusions by the five methods. (**B**) The percentages of V(D)J recombinations in fusions detected by the five methods. (**C**) The expressions of *SLC4A10* shown in the tSNE plot of all T cells. (**D**) The cells with *TRAJ33-TRAV1-2* and *TRAJ12-TRAV1-2* colored in the tSNE plot. (**E,F**) The barplots of numbers of cells with the *TRAJ33-TRAV1-2* (E) and *TRAJ12-TRAV1-2* (F) recombinations by different algorithms.

Figure 6. The MM scRNA-seq data. (**A**) The number of detected gene fusions by the five methods. (**B**)The percentage of IgH-related fusions in fusions detected by the five methods. (**C**) The tSNE plot the all MM single cells. The cells with two *IgH-WHSC1* fusions are colored in the plot. The cells from patient RMM2 and SMM0 are marked by triangle and rectangle, respectively. (**D**) The expression of *WHSC1* shown in the tSNE plot. (**E**) The mean read depth of *WHSC1* at different locations for the cells with the two *IgH-WHSC1* fusions and the cells without the fusions. The black triangles indicate the breakpoints of the two fusions. The supporting number of splicing junctions are also shown in the plot (the numbers above the arcs). The read depth of a single cell at a location is calculated as the number of reads covering the location per million. The mean read depth is the average depth of all cells in a group. (**E**) The barplots of numbers of cells with the *IgH-WHSC1* fusions by different algorithms.

Table 1. The contingency table between the *TRAJ33-TRAV1-2/TRAJ12-TRAV1-2* fusion and the expression of *SLC4A10*. The high expression are the cells whose *SLC4A10* expression is greater than 1 and the low expression are other cells. The Fisher's exact test gives a p-value smaller than 10^{-16}.

	TRAJ33-TRAV1-2/ TRAJ12-TRAV12	Other
High Expression	108	90
Low Expression	40	2117

Figure S1. Number of fusion candidates after applying different filters for the (**A**) spike-in data, (**B**) T cell data and (**C**) MM data. The top is the total number of fusion candidates, and the second layer is the number of fusion candidates excluding pseudogenes, lncRNAs, genes without an approved symbol, and candidates in intronic regions (they are called pseudogene-, lncRNA-, no-approved-symbol- and intron- filters). The third layer is the number of candidates supported by at least 2 cells. The fourth layer shows the numbers of fusion candidates remained after the filtering by the statistical model and the deep learning model, respectively. The fifth layer is the number of candidates that pass both models. The last number indicates the number of output fusions after removing candidates whose number of supporting discordant reads is ten times more than supporting split-mapped reads (too-many-discordant-filter) and candidates with a partner gene involving in more than five fusion candidates (too-many-partner-filter).

Figure S2. Statistics of chimeric reads. The boxplots of (**A**) the total number of chimeric reads, (**B)** the proportions of chimeric reads in all mapped reads and (**C**) the total number of mapped reads in different scRNA-seq data.

Figure S3. The bi-LSTM model. (**A**) The design of the bi-LSTM. (**B**)The ROCs and (**C**) PR curves of the Bi-LSTM without retraining.

Figure S4. Performance of CNN model. (**A**) The design of the CNN model (**B**) The ROCs of the CNN model for different single cell data sets. The AUCs are also shown. (**C**) The PR curves and their AUPRs of the CNN model. (**D**) The densities of the technical artefact score of gene fusions in the PCAWG study by the CNN models retrained using six different datasets. (**E**) The densities of the technical artefact score of chimeric reads. The models are retrained using different datasets.

Figure S5. The precisions and recalls of scFusion and four bulk methods in six different simulation setups. The figures in the two rows correspond to simulations with 500 cells and 1000 cells, and the figures in the three columns correspond to simulations with 2 million, 3 million and 4 million reads in each data. The dots in the figures are the means of precisions and recalls of ten simulations in each setup and the boxes ±1 standard deviation (SD) of the precisions and recalls. The dashed lines are the contour lines with constant F-scores (F-scores are marked in the top-left figure).

Figure S6. The detection powers of fusions at different expression levels using (**A**) 500 and (**B**) 1000 cells.

Figure S7. (**A**) The design of the five spike-in fusion genes. In each panel, the original partner genes are shown at the top and the fusion genes are shown at the bottom. The scissors represent the breakpoints of the fusions and the local sequences are shown below the genes and the fusion genes. (**B**) The percentage of reported gene fusions having supporting reads in bulk data.

Figure S8. Fusions are correlated with gene up-regulations. (**A**) The volcano plots of the differential expression analysis of T cells between cells with and without the *TRAJ33-TRAV1-2* or *TRAJ12-TRAV1-2* recombination. (**B**) The *SLC4A10* expression is significantly higher in cells with the *TRAJ33-TRAV1-2* or *TRAJ12-TRAV1-*2 recombination than other cells. (**C**) The volcano plots of the differential expression analysis of T cells between cells with and without the *IgH-WHSC1* fusion. (**D**) The local view of the mean read depth of *WHSC1* at different locations for the cells with the two *IgH-WHSC1* fusions and the cells without the fusions. (**E**) The expression of *CCND1* shown in the tSNE plot. (**F**) The expression of *FRZB* shown in the tSNE plot.

Figure S9. Differential expresseion analysis. The expression of *ALPK1*, *TIFA, TRAJ33* and *TRAJ12* in the two cell groups.

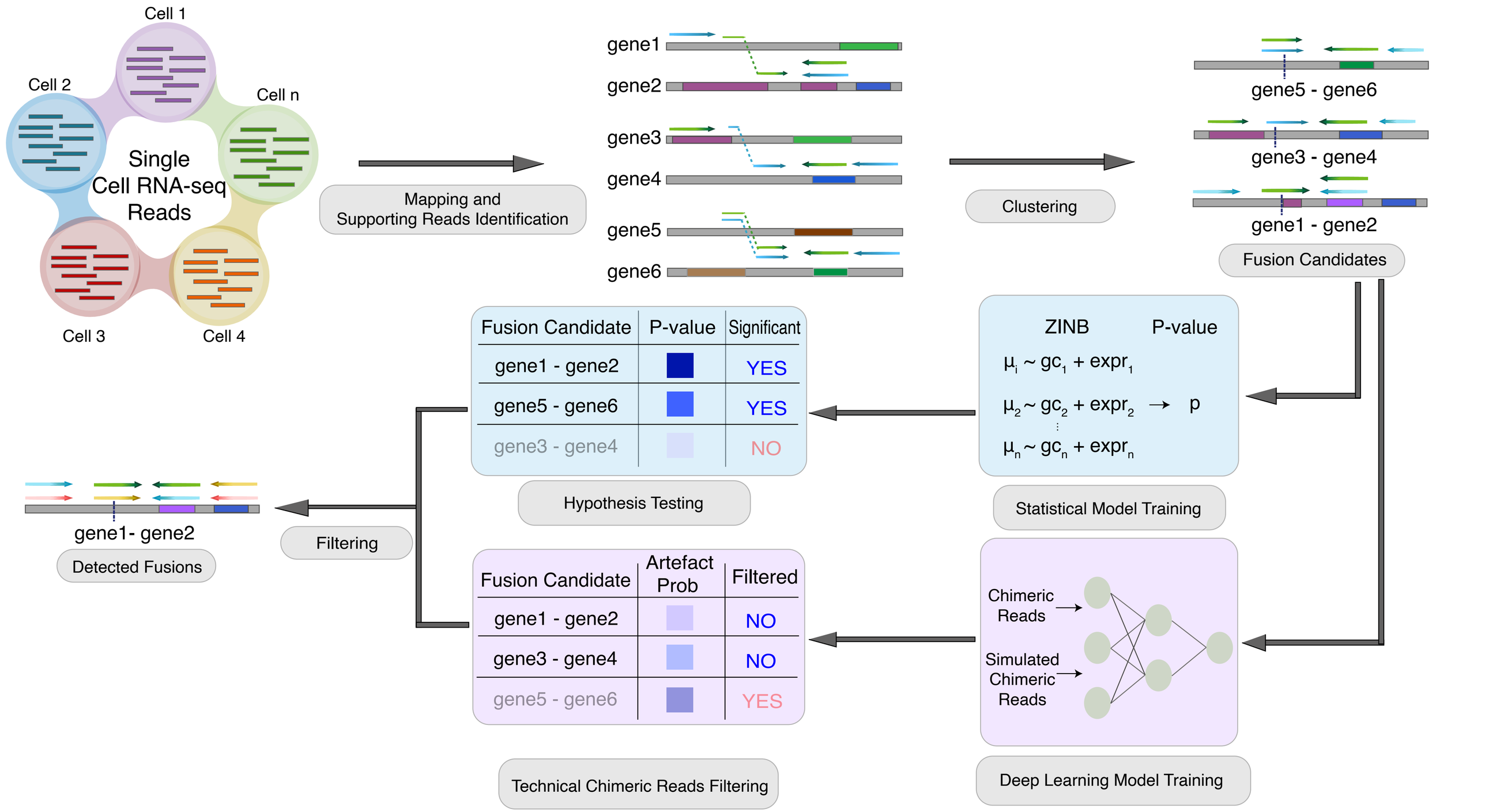
Cell 1
Cell 2
Cell n
Single Cell RNA-seq Reads
Cell 3
Cell 4
Mapping and Supporting Reads Identification
gene1
gene2
gene3
gene4
gene5
gene6
Clustering
gene5 - gene6
gene3 - gene4
gene1 - gene2
Fusion Candidates
ZINB
P-value
$\mu_i \sim gc_1 + expr_1$
$\mu_2 \sim gc_2 + expr_2$
$\mu_n \sim gc_n + expr_n$
p
Statistical Model Training
Fusion Candidate | P-value | Significant
gene1 - gene2 | YES
gene5 - gene6 | YES
gene3 - gene4 | NO
Hypothesis Testing
Chimeric Reads
Simulated Chimeric Reads
Deep Learning Model Training
Fusion Candidate | Artefact Prob | Filtered
gene1 - gene2 | NO
gene3 - gene4 | NO
gene5 - gene6 | YES
Technical Chimeric Reads Filtering
Filtering
gene1- gene2
Detected Fusions

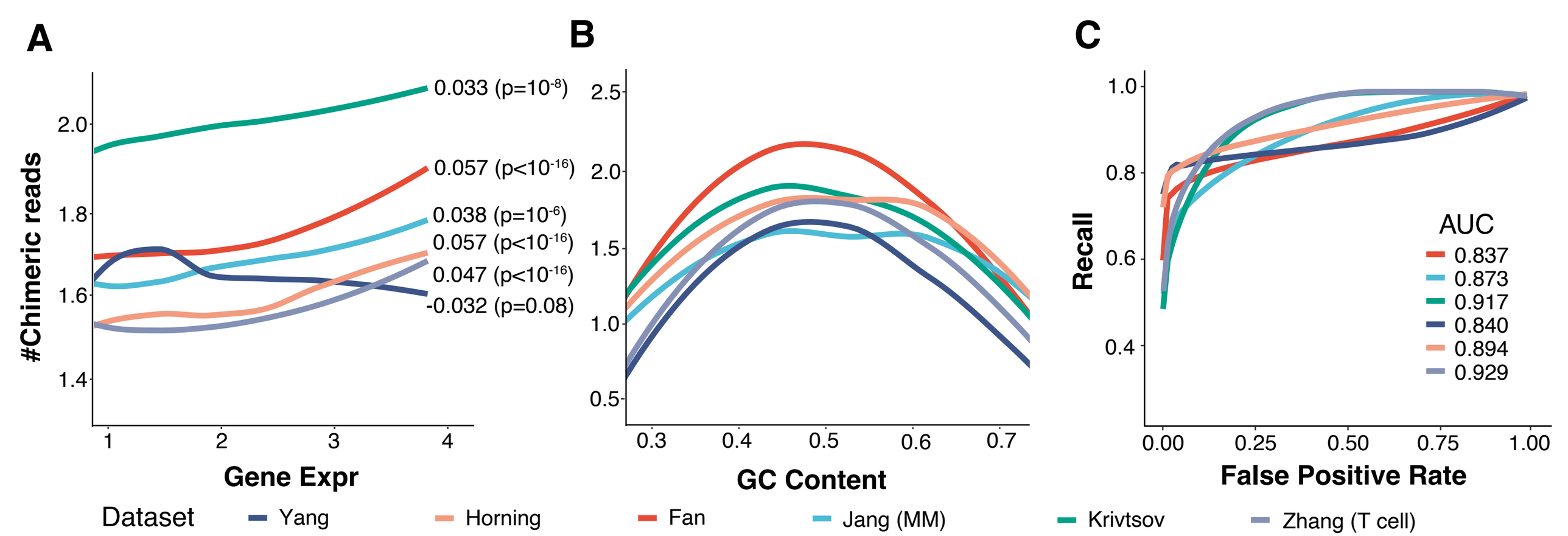
A
#Chimeric reads
Gene Expr
0.033 (p=10^-8)
0.057 (p<10^-16)
0.038 (p=10^-6)
0.057 (p<10^-16)
0.047 (p<10^-16)
-0.032 (p=0.08)
B
GC Content
C
Recall
False Positive Rate
AUC
0.837
0.873
0.917
0.840
0.894
0.929
Dataset
Yang
Horning
Fan
Jang (MM)
Krivtsov
Zhang (T cell)
D
Precision
Recall
AUPR
0.893
0.873
0.921
0.904
0.928
0.940
E
Score densities for PCAWG fusions
Density
Probability
F
Score densities for chimeric reads
Density
Probability

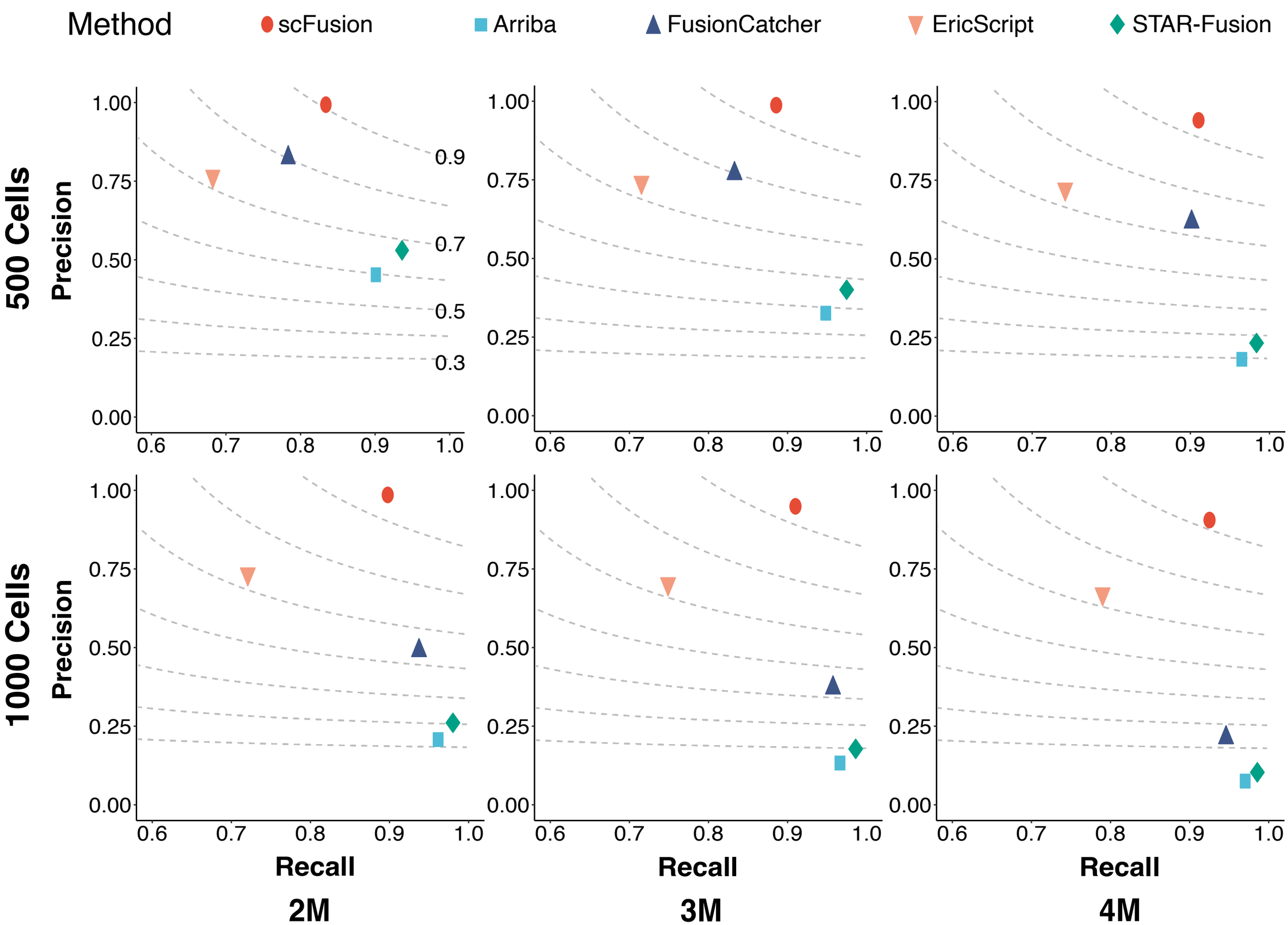
Method
scFusion
Arriba
FusionCatcher
EricScript
STAR-Fusion
500 Cells
1000 Cells
Precision
Recall
0.9
0.7
0.5
0.3
1.00
0.75
0.50
0.25
0.00
0.6
0.7
0.8
0.9
1.0
2M
3M
4M

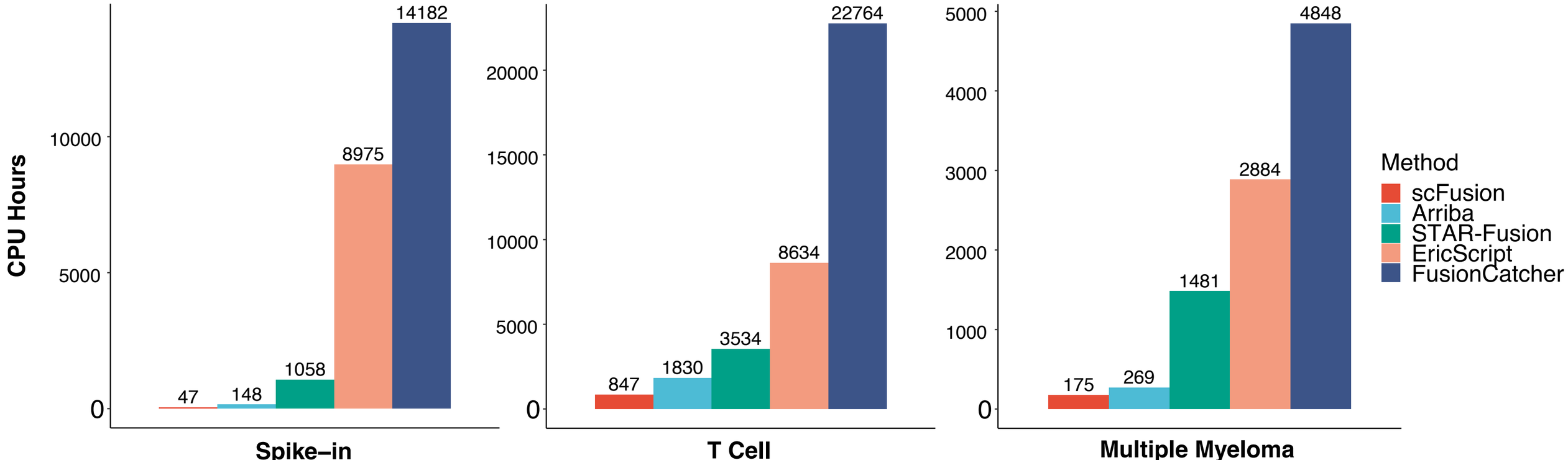
CPU Hours
0
5000
10000
47
148
1058
8975
14182
Spike–in
0
5000
10000
15000
20000
847
1830
3534
8634
22764
T Cell
0
1000
2000
3000
4000
5000
175
269
1481
2884
4848
Multiple Myeloma
Method
scFusion
Arriba
STAR-Fusion
EricScript
FusionCatcher

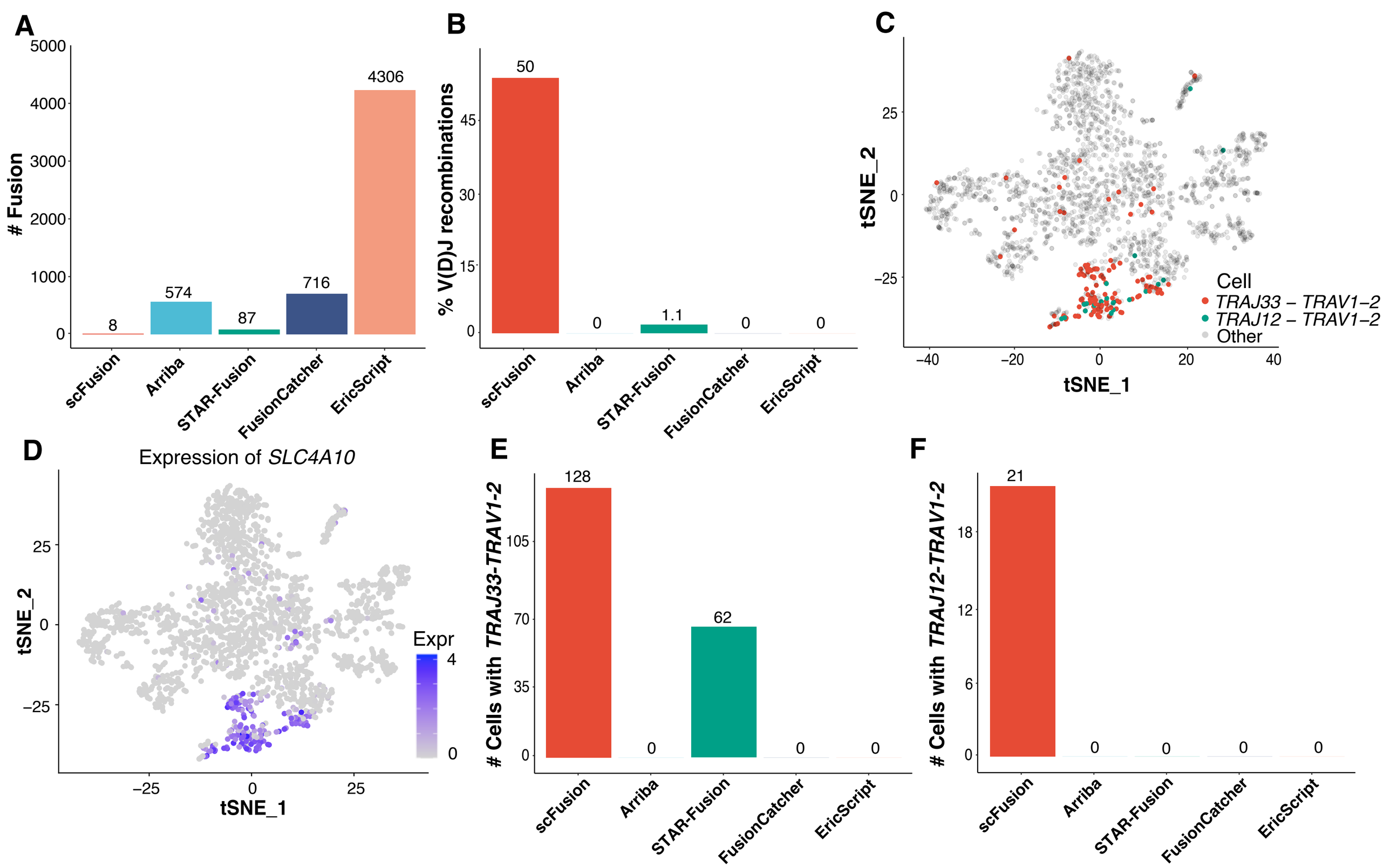
A
Fusion
5000
4000
3000
2000
1000
0
8
574
87
716
4306
scFusion
Arriba
STAR-Fusion
FusionCatcher
EricScript
B
% V(D)J recombinations
45
30
15
0
50
0
1.1
0
0
scFusion
Arriba
STAR-Fusion
FusionCatcher
EricScript
C
tSNE_2
25
0
−25
tSNE_1
−40
−20
0
20
40
Cell
TRAJ33 – TRAV1−2
TRAJ12 – TRAV1−2
Other
D
Expression of SLC4A10
tSNE_2
25
0
−25
tSNE_1
−25
0
25
Expr
4
0
E
Cells with TRAJ33-TRAV1-2
105
70
35
0
128
0
62
0
0
scFusion
Arriba
STAR-Fusion
FusionCatcher
EricScript
F
Cells with TRAJ12-TRAV1-2
18
12
6
0
21
0
0
0
0
scFusion
Arriba
STAR-Fusion
FusionCatcher
EricScript

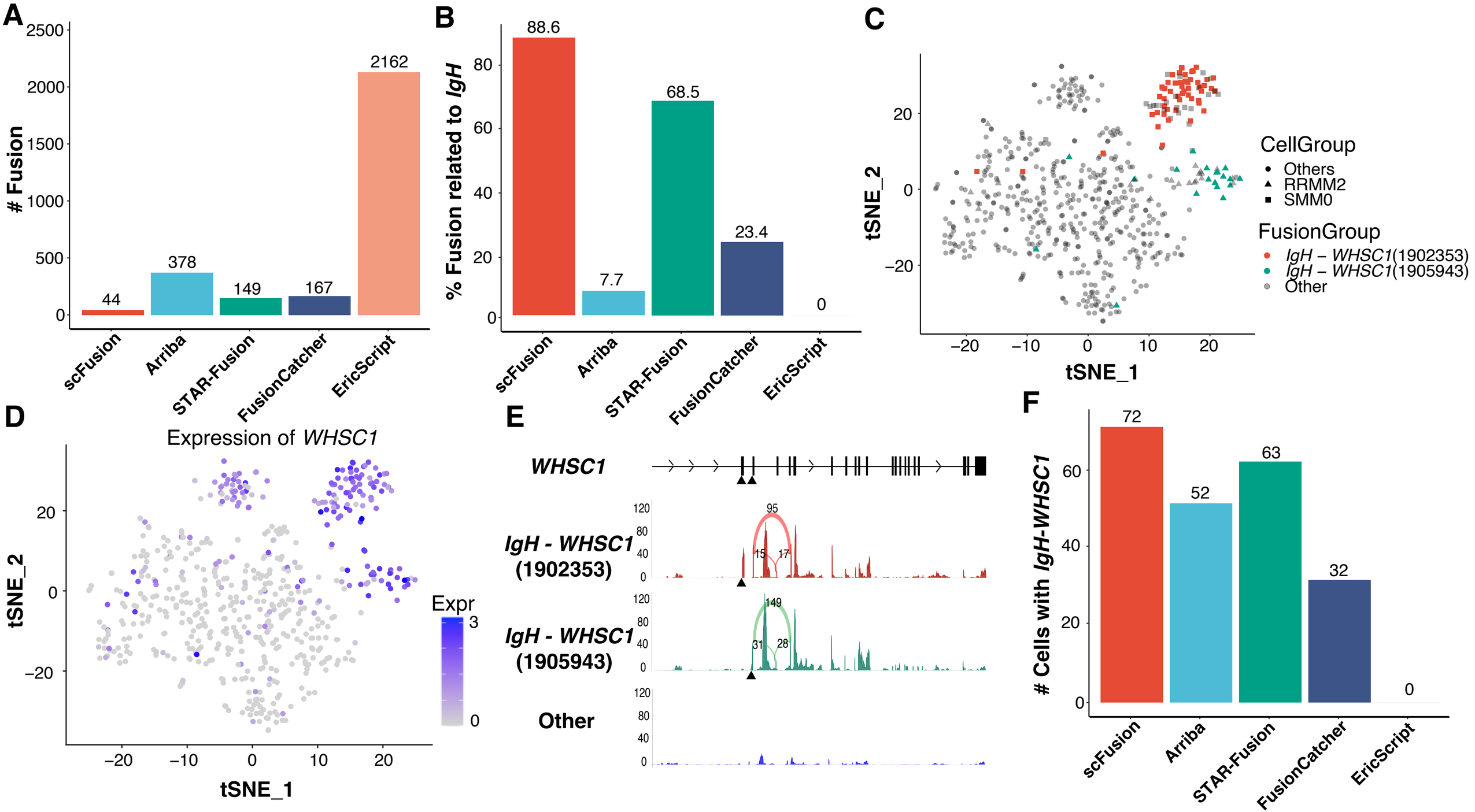
A
Fusion
2500
2000
1500
1000
500
0
44
378
149
167
2162
scFusion
Arriba
STAR-Fusion
FusionCatcher
EricScript
B
% Fusion related to IgH
88.6
7.7
68.5
23.4
0
C
tSNE_2
tSNE_1
CellGroup
Others
RRMM2
SMM0
FusionGroup
IgH – WHSC1(1902353)
IgH – WHSC1(1905943)
Other
D
Expression of WHSC1
Expr
3
0
E
WHSC1
IgH - WHSC1 (1902353)
IgH - WHSC1 (1905943)
Other
95
15
17
149
31
28
F
Cells with IgH-WHSC1
72
52
63
32
0

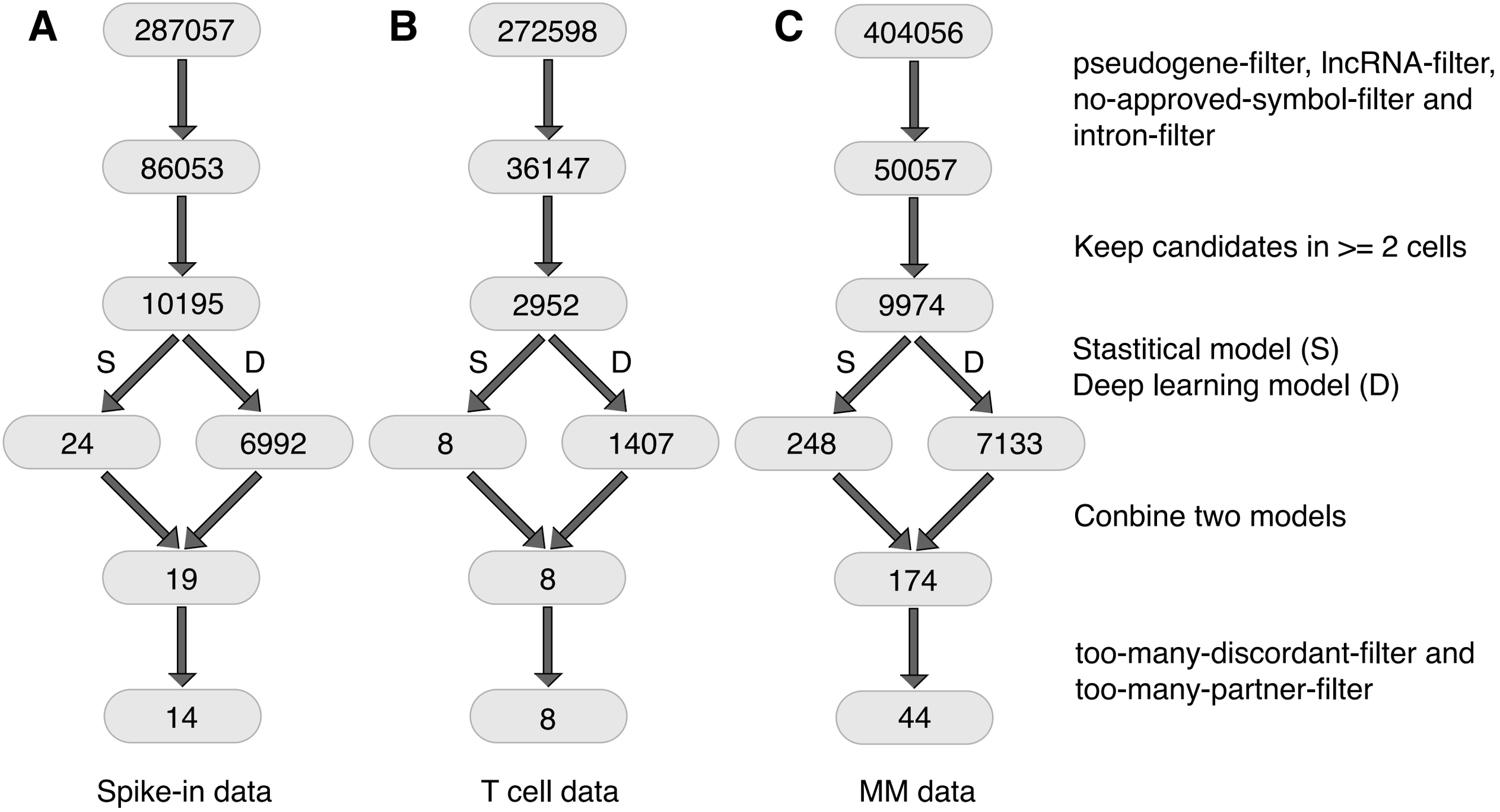
A
287057
86053
10195
S
D
24
6992
19
14
Spike-in data
B
272598
36147
2952
S
D
8
1407
8
8
T cell data
C
404056
50057
9974
S
D
248
7133
174
44
MM data
pseudogene-filter, lncRNA-filter, no-approved-symbol-filter and intron-filter
Keep candidates in >= 2 cells
Stastitical model (S)
Deep learning model (D)
Conbine two models
too-many-discordant-filter and too-many-partner-filter

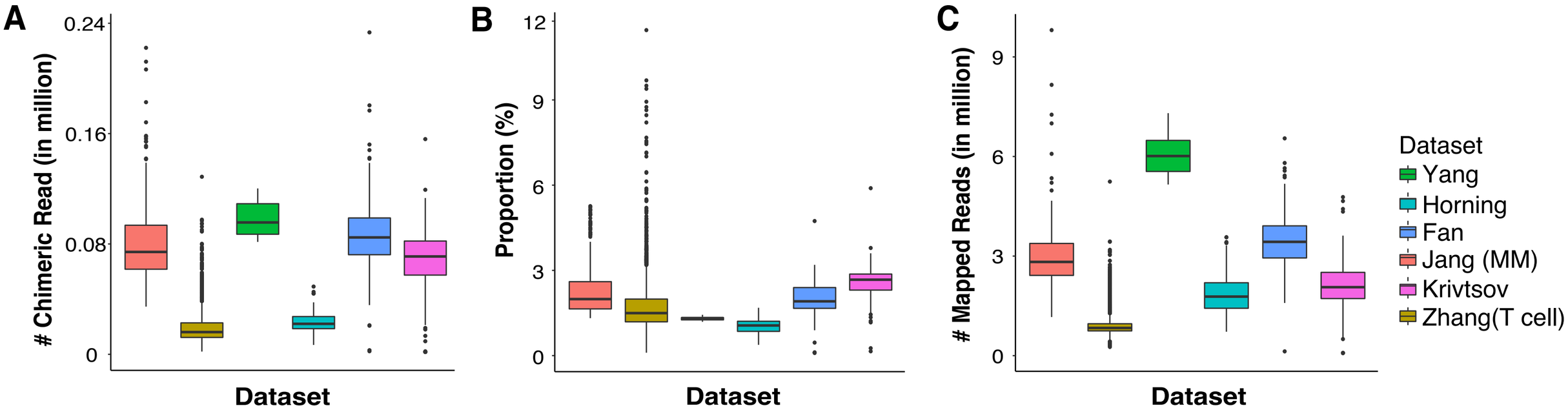
A
0.24
0.16
0.08
0
Chimeric Read (in million)
Dataset
B
12
9
6
3
0
Proportion (%)
Dataset
C
9
6
3
0
Mapped Reads (in million)
Dataset
Dataset
Yang
Horning
Fan
Jang (MM)
Krivtsov
Zhang(T cell)

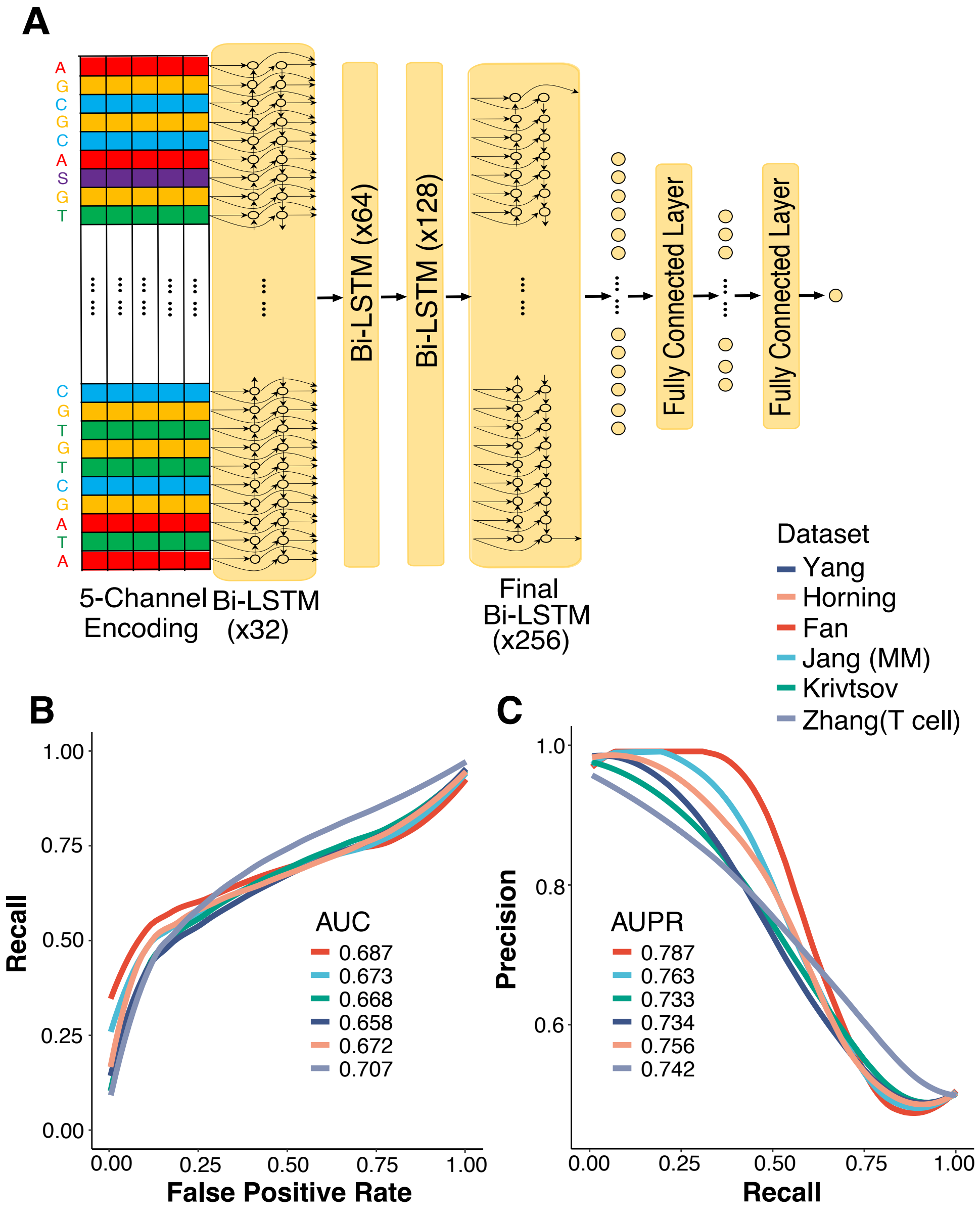
A
5-Channel Encoding
Bi-LSTM (x32)
Bi-LSTM (x64)
Bi-LSTM (x128)
Final Bi-LSTM (x256)
Fully Connected Layer
Fully Connected Layer
Dataset
Yang
Horning
Fan
Jang (MM)
Krivtsov
Zhang(T cell)
B
Recall
False Positive Rate
AUC
0.687
0.673
0.668
0.658
0.672
0.707
C
Precision
Recall
AUPR
0.787
0.763
0.733
0.734
0.756
0.742

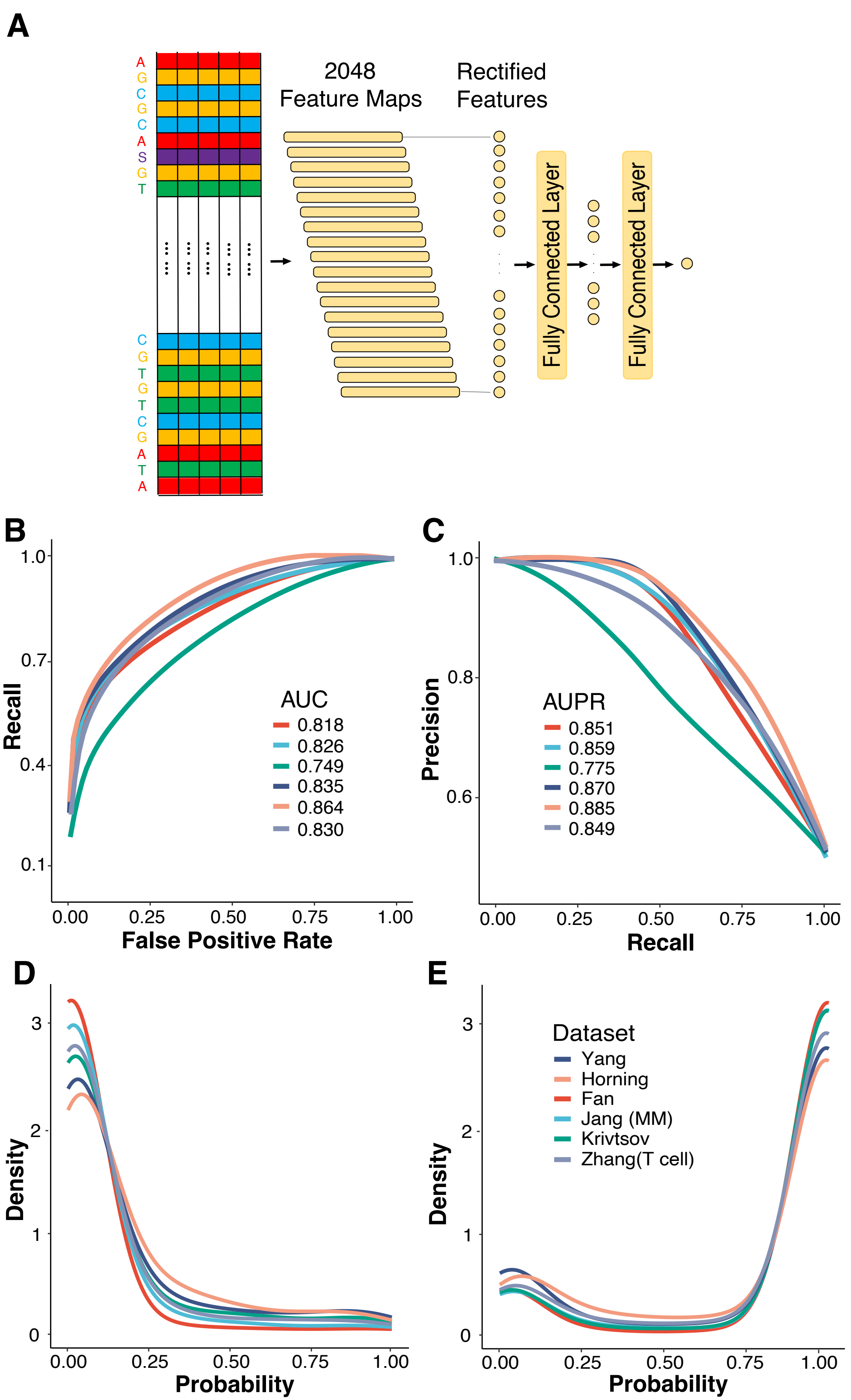
A
2048
Feature Maps
Rectified
Features
Fully Connected Layer
Fully Connected Layer
B
Recall
False Positive Rate
AUC
0.818
0.826
0.749
0.835
0.864
0.830
C
Precision
Recall
AUPR
0.851
0.859
0.775
0.870
0.885
0.849
D
Density
Probability
E
Density
Probability
Dataset
Yang
Horning
Fan
Jang (MM)
Krivtsov
Zhang(T cell)

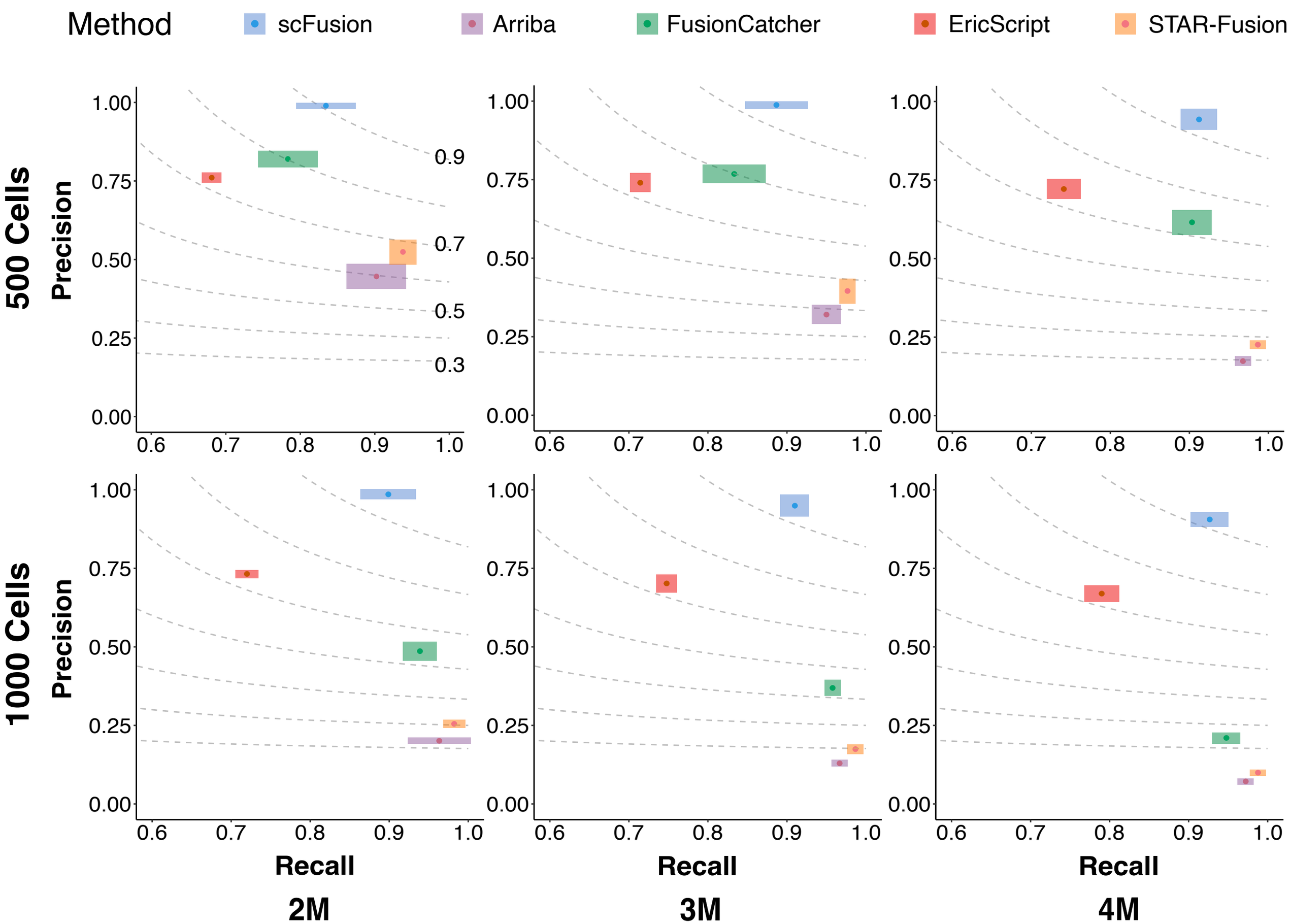
Method
scFusion
Arriba
FusionCatcher
EricScript
STAR-Fusion
500 Cells
1000 Cells
Precision
Recall
0.9
0.7
0.5
0.3
1.00
0.75
0.50
0.25
0.00
0.6
0.7
0.8
0.9
1.0
2M
3M
4M

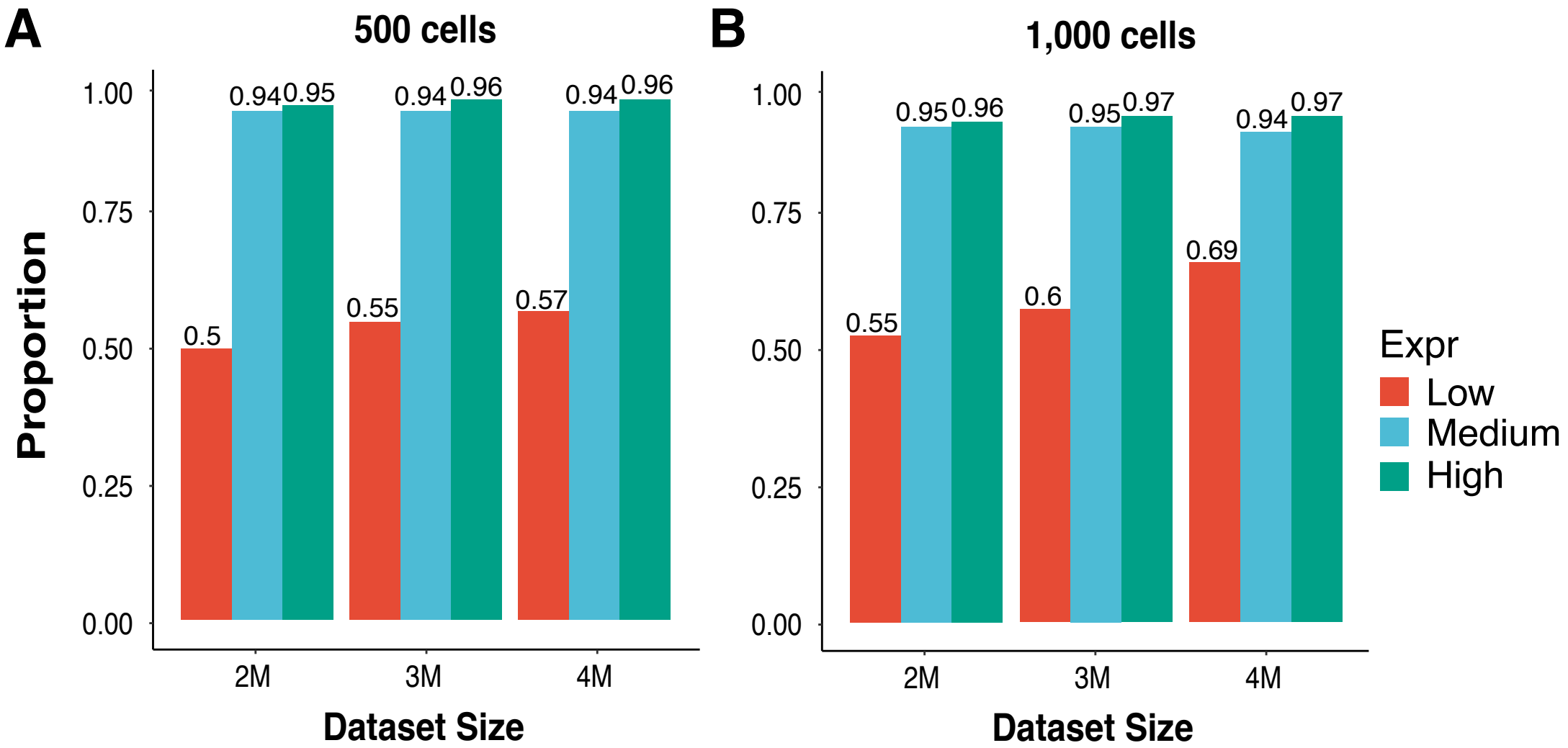
A
500 cells
B
1,000 cells
Proportion
1.00
0.75
0.50
0.25
0.00
0.5
0.94
0.95
0.55
0.94
0.96
0.57
0.94
0.96
0.55
0.95
0.96
0.6
0.95
0.97
0.69
0.94
0.97
2M
3M
4M
Dataset Size
Expr
Low
Medium
High

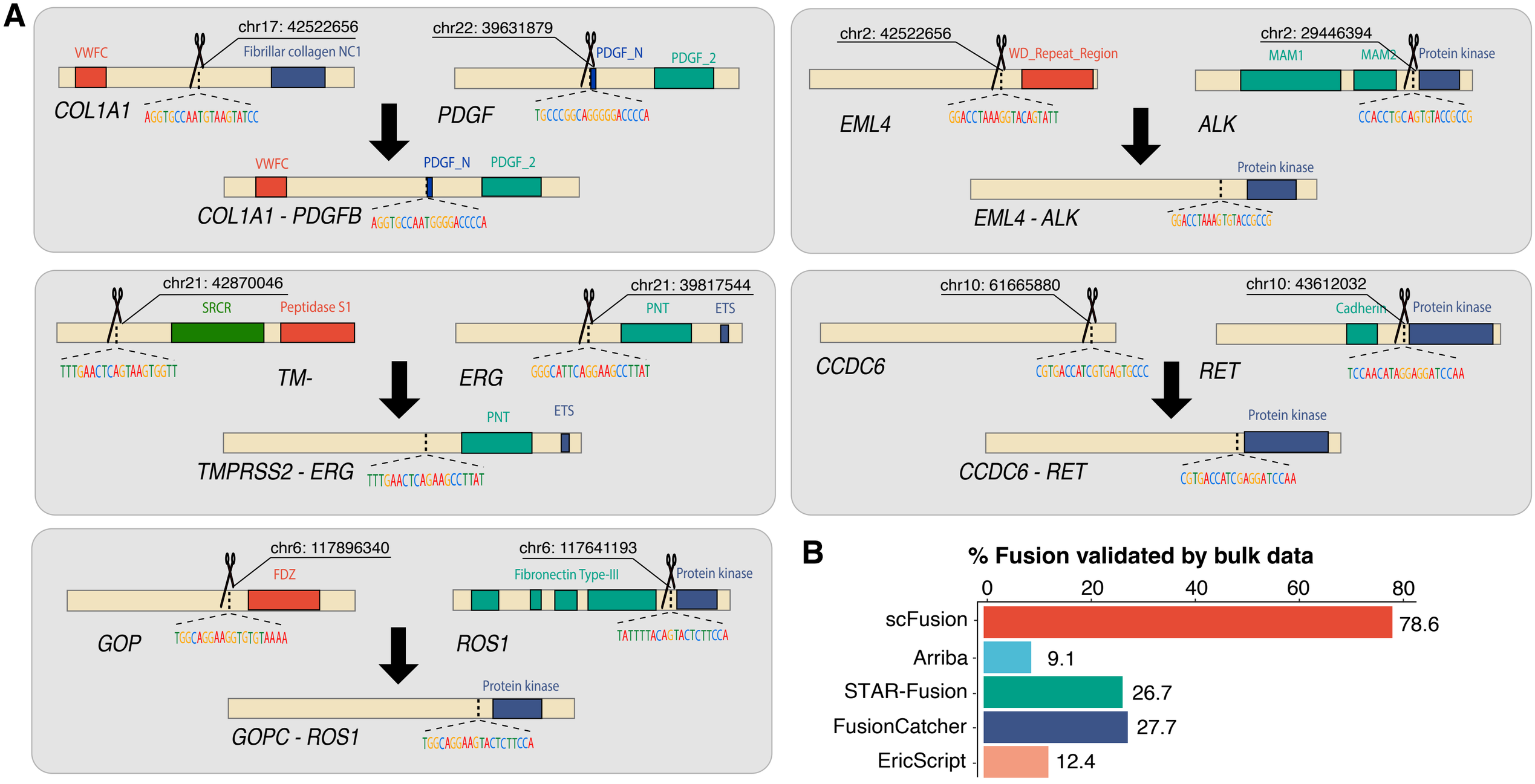
A
chr17: 42522656
VWFC
Fibrillar collagen NC1
COL1A1
AGGTGCCAATGTAAGTATCC
chr22: 39631879
PDGF_N
PDGF_2
PDGF
TGCCCGGCAGGGGGACCCCA
VWFC
PDGF_N
PDGF_2
COL1A1 - PDGFB
AGGTGCCAATGGGGACCCCA
chr2: 42522656
WD_Repeat_Region
EML4
GGACCTAAAGGTACAGTATT
chr2: 29446394
MAM1
MAM2
Protein kinase
ALK
CCACCTGCAGTGTACCGCCG
Protein kinase
EML4 - ALK
GGACCTAAAGTGTACCGCCG
chr21: 42870046
SRCR
Peptidase S1
TTTGAACTCAGTAAGTGGTT
TM-
chr21: 39817544
PNT
ETS
ERG
GGGCATTCAGGAAGCCTTAT
PNT
ETS
TMPRSS2 - ERG
TTTGAACTCAGAAGCCTTAT
chr10: 61665880
CCDC6
CGTGACCATCGTGAGTGCCC
chr10: 43612032
Cadherin
Protein kinase
RET
TCCAACATAGGAGGATCCAA
Protein kinase
CCDC6 - RET
CGTGACCATCGAGGATCCAA
chr6: 117896340
FDZ
GOP
TGGCAGGAAGGTGTGTAAAA
chr6: 117641193
Fibronectin Type-III
Protein kinase
ROS1
TATTTTACAGTACTCTTCCA
Protein kinase
GOPC - ROS1
TGGCAGGAAGTACTCTTCCA
B
% Fusion validated by bulk data
0
20
40
60
80
scFusion
78.6
Arriba
9.1
STAR-Fusion
26.7
FusionCatcher
27.7
EricScript
12.4

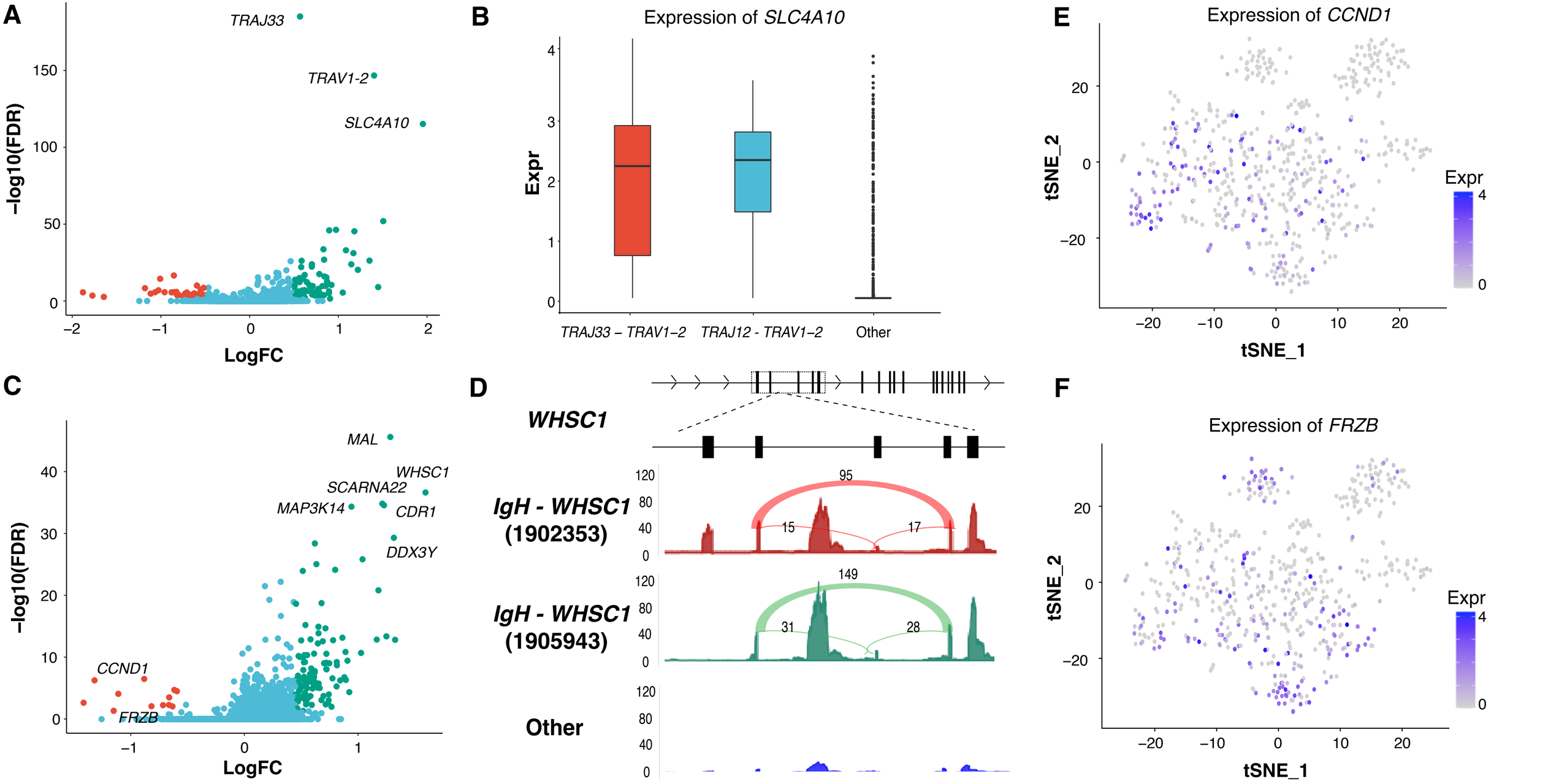
A
TRAJ33
TRAV1-2
SLC4A10
−log10(FDR)
LogFC
B
Expression of SLC4A10
Expr
TRAJ33 – TRAV1–2
TRAJ12 - TRAV1–2
Other
E
Expression of CCND1
tSNE_2
tSNE_1
Expr
C
MAL
WHSC1
SCARNA22
MAP3K14
CDR1
DDX3Y
CCND1
FRZB
−log10(FDR)
LogFC
D
WHSC1
IgH - WHSC1 (1902353)
95
15
17
IgH - WHSC1 (1905943)
149
31
28
Other
F
Expression of FRZB
tSNE_2
tSNE_1
Expr

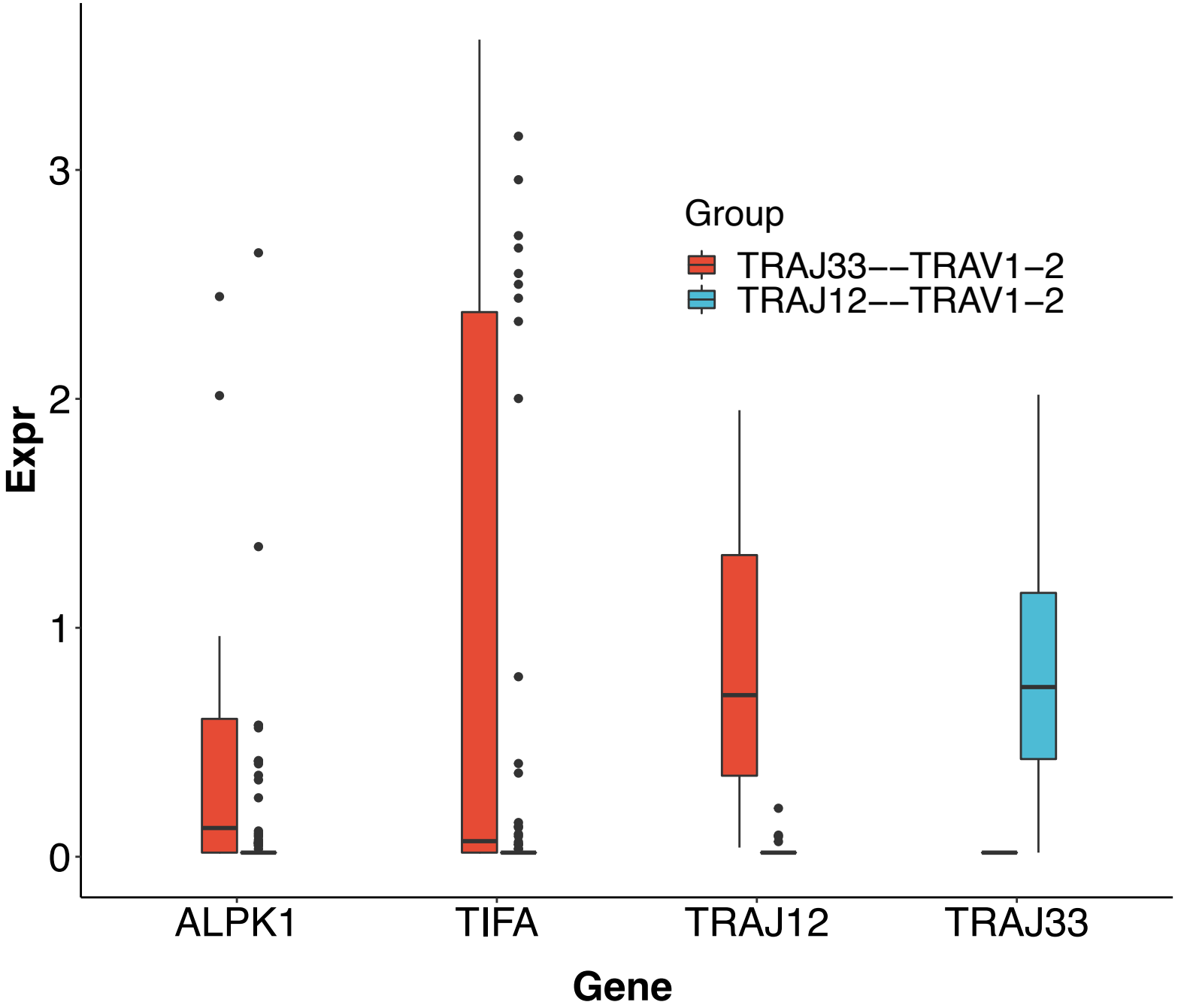
Group
TRAJ33−−TRAV1−2
TRAJ12−−TRAV1−2
Expr
0
1
2
3
ALPK1
TIFA
TRAJ12
TRAJ33
Gene